POLITECNICO DI TORINO

Master Thesis in Electrical Engineering

Single- and Three-phase on-board charger for Electric Vehicle

Author: Marco Roberto De Cesero

Supervisor: Prof. Gianmario Pellegrino

Advisor: Paolo Pescetto

July 2020

Contents

1 Introduction **4**

1.1 Classification of battery chargers 5

1.2 Standards requirements 7

1.3 Topologies of battery chargers 8

1.4 Specifications of the project 12

1.5 Proposed solution 14

2 Analysis of the proposed structure **17**

2.1 The unidirectional T-type converter 17

2.1.1 Single-phase T-type converter 19

2.1.2 Cascaded current and voltage control loops 21

2.1.3 The Discontinuous Conduction Mode 24

2.1.4 Interleaved single-phase T-type converter and current control with phase interleaving 24

2.1.5 Control strategy for unidirectional three-phase T-type converter 27

2.1.6 PLL scheme for single-phase T-type converter 30

2.1.7 PLL scheme for three-phase T-type converter 34

2.2 LLC converter 36

2.2.1 First Harmonic Approximation 36

2.2.2 Voltage transfer function of the LLC converter 39

2.2.3 Zero Voltage Switching 43

2.2.4 The equivalent input impedance 46

2.2.5 Step-up and Step-down functioning 48

2.2.6 Control strategy for the LLC converter 50

3 Preliminary design of the battery charger **57**
3.1 Design of the T-type converter 57
3.1.1 Design of the output capacitors 58
3.1.2 Design of the input inductors 59
3.1.3 Choice of the semiconductor devices 62
3.2 Design of the LLC converter 63
3.2.1 Design of the resonant tank 63
3.2.2 Design of the resonant inductor 67
3.2.3 Transformer design 71
3.2.4 Output filter 74

4 Software simulation **75**
4.1 Simulation of the T-type converter 75
4.1.1 Three-phase configuration 76
4.1.2 Single-phase configuration 78
4.2 Simulation of the LLC converter 80
4.3 Choice of the commercial components 85
4.4 Simulation of the complete converter 87
4.5 Simulation of the ZVS in the LLC converter 88

5 Evaluation of weight, volume and losses **97**
5.1 Rendering of the battery charger 97
5.2 Evaluation of the power losses 98
5.2.1 Power losses of the T-type converter 100
5.2.2 Power Losses of the LLC converter 100
5.3 Efficiency of the battery charger 104
5.4 Comparison with a commercial solution 105

6 Conclusion **107**

Bibliography **109**

Acknowledgements

This thesis has been conducted with the support of Power Electronics Innovation Center of Politecnico di Torino.

This thesis has been developed under the FITGEN project, which has received funding from the European Unions H2020 research and innovation programme under Grant Agreement no. 824335.

Abstract

The main goal of this master thesis is developing a preliminary design and sizing of an on-board battery charger for an A-segment road electric vehicle, pursuing high efficiency and flexibility. The work is part of the FITGEN (Functionally Integrated e-axle ready for mass market Third GENeration electric vehicles) project, founded by European Unions H2020 research and innovation programme under Grant Agreement no. 824335.

The considered architecture is composed by two stages: a T-type converter as AC/DC stage and a LLC converter as DC/DC stage. In order to make the battery charger as adaptable as possible, both three- and single-phase supply system has been considered during the design, leading to a structure that can be used both in three- and single-phase configuration without changing in the internal components.

This master thesis is divided into the following chapters:

1. Introduction: analysis of the type of the battery charger and explanation of the proposed structure

2. Battery charger description: accurate analysis of the T-type and LLC conveter and of their control strategies

3. Preliminary design: describes the method used for choosing the components of the two converters

4. Simulation results: demonstrate the feasibility of the proposed design and control strategy

5. Evaluation of weight, volume and losses: gives a first rendering of the complete battery charger and a first analysis of power losses and efficiency. The proposed

solution is then compared with a commercial battery charger

6. Conclusion

Chapter 1

Introduction

Nowadays the market of Electric Vehicle (EV) is increasing day by day and the research is making efforts find a solution for all the demand.

The actual state of art of UltraFast Charger (UFC) permits to recharge a battery pack in a reasonable time, giving a sufficient driving range for the user. Anyway, the UFC Stations are not yet widely distributed in most of the countries to recharge an Electrical Vehicle. Moreover, at the moment there is not a unique standard defining the charging voltage, current and communication protocol between the UFC and the Battery Management System (BMS) of the EV.

Nowadays there are three chager power levels ways to recharge a battery pack [1]:

1. Level 1 charging: it is the slowest method and the input configuration is normally single-phase

2. Level 2 charging: it is the primary method for dedicated private and public facilities. The input configuration can be both single- or three-phase

3. Level 3 charging: it is the fastest method and it requires off-board battery charger, which are installed in public dedicated areas. The input configuration is three-phase

Considering the level 1 and level 2 charging methods, the input configuration can be both single- and three-phase. So a good solution is to use a three- phase structure

that can be reconfigured when fed by single phase inlet to a single-phase supply. In this way, customers don't need to worry about how and where to recharge their vehicle.

It is not worthless to note also that improving the charging efficiency will affect the cost saving of the customers and for this reasons, lot of manufactures are spending efforts in order to improve the quality of battery chargers.

Another problem about on-board chargers is related to the possibility of recharging in different grid configurations, avoiding the customer to think about where he can recharge his battery pack.

There are two different grid configurations, single-phase and three-phase system, normally the latter is used for the transmissions of high power levels while the other one is used for lower power levels. So a good characteristic that a battery charger should have is the possibility to connect to both of these systems, depending on the situation. Considering that in an EV weight and volume are obviously two of the most important aspects in the design of the vehicle components, a good idea is to find a solution that can use the same components in different situations. In this way charging the battery pack doesn't need a high number of components, even if the recharge is accomplished in different supply configurations.

1.1 Classification of battery chargers

Typically, a on-board charger (OBC) is essentially composed of two power converters as shown in Figure 1.1.

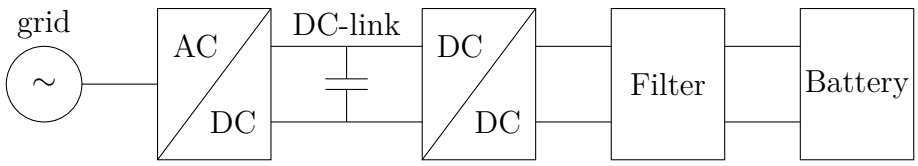

Figure 1.1: Parts of the battery charger

The first element is AC/DC converter that is connected to the grid and it normally has the function to maintain the electrical quantities on the grid side to specific standards and to convert them to a DC form. Subsequently, the electrical quantities driven through the DC link, are regulated by a DC/DC converter,

which is connected to the battery pack. In some cases there is a filter between the DC/DC converter and the battery pack that permits a better quality of the electrical quantities at the battery pack input.

Due to the variety of existing power converters, the actual state of the art concerning battery chargers is characterized by a huge number of different solutions, but there are some aspects that permits to classify them.

The first classification has been already cited before and it concerns the kind of supply system: three-phases or single-phase system. As the first step of a battery charger is the AC/DC conversion, three-phases configurations allow some advantages over the single-phase ones, such:

- lower ripple factor at DC side
- smaller filtering components
- higher power transmission

However, a three-phase supply system is not available everywhere, so also single-phase configurations must be considered.

A second classification depends on the directions that the power flow can take, distinguishing unidirectional from bidirectional chargers. In unidirectional converters the power can flow just from the supply to the battery, while in bidirectional converter the power can flow in both the directions (Figure 1.2)

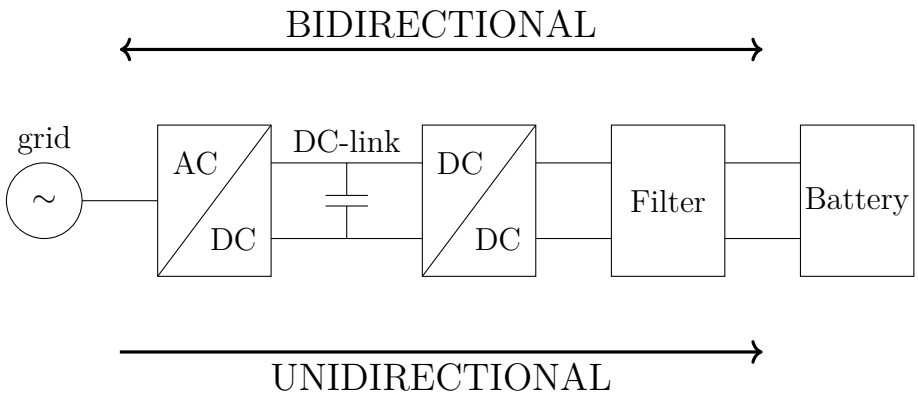

Figure 1.2: Unidirectional and bidirectional converters

A recent trend in research, at tne moment not commonly adopted in practice, is evaluating the possibility of using the energy stored in EVs battery packs to

stabilize the grid in which they are connected to. This implies that electrical power must be able to flow both from grid to battery pack and vice versa, from battery pack to grid. Anyway, not all the manufactures adopted this solution yet as the unidirectional converters are normally cheaper and more compact respect to the bidirectional counterparts.

There is also a classification between High Frequency (HF) and Low Frequency (LF) solutions. In both cases the battery charger must provide a galvanic isolation between battery pack and grid using a power transformer. HF solutions have normally the transformer as part of the DC/DC converter and their use introduces many advantages such as smaller weight and volumes and higher power density. One of the main problems related to HF converters is the control complexity. On the other side, LF solutions are characterized by a LF transformer, which is bigger than the HF one, but it permits using a simpler DC/DC converter, reducing its cost and complexity.

Depending on the connection to the drivetrain, the OBCs can be classified in independent or combined (integrated) topologies [2]. In the integrated OBC, the drivetrain elements are used as battery chargers components during the recharge process. This leads to a reduces number of components of the electric vehicle and space saving.

1.2 Standards requirements

As the battery charger is connected to the grid it must satisfy the standard requirements. The standard that have been taken into account for this work are reported in [3], which impose the requirements for battery charger with a nominal voltage up to 1000Vac or 1500Vdc.

As the charger is connected to the grid when the battery is charging, important requirements about power quality must be satisfied. The harmonics levels on the input current that the standards imposes are based on the input current values itself (Table 1.1, Table 1.2).

Harmonic number N	Maximum authorized current A
Odd harmonics	
3	2.3
5	1.14
7	0.77
9	0.4
11	0.33
13	0.21
$15 \leq n \leq 39$	0.15·15/n
Even harmonics	
2	1.08
4	0.43
6	.3
$8 \leq n \leq 40$	0.23·8/n

Table 1.1: Maximum allowed harmonics for $I_i \leq 16A$

Acceptable individual harmonic current $I_n/I_1\%$						maximum harmonic ratio
I_3	I_5	I_5	I_5	I_{11}	I_{13}	THD
21.6	10.7	7.2	3.8	3.1	2	23

Table 1.2: Acceptable harmonics for $16A < I_i \leq 75A$

1.3 Topologies of battery chargers

In order to choose a good solution for the battery charger configuration, it is possible to split the discussions in two parts: the first one talks about the front-end converter (AC/DC) while the second one is dedicated to the DC/DC converter.

Considering that the AC/DC converter must perform also as Power Factor Correction (PFC), the easiest existing configuration is the single-phase boost PFC [4]. It is composed of an input diode rectifier that rectifies the input voltage, followed by a normal boost converter, which has the function of improving the Power Factor seen from the grid.

The advantage of this configuration is that presents few switching elements if

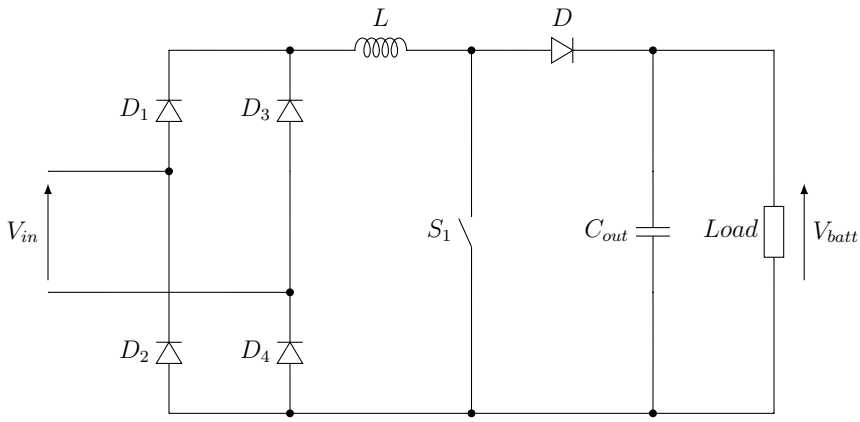

Figure 1.3: Single-phase boost PFC

compared with other configurations and it is very easy to control. Anyway, it does not allow high flexibility if different supply systems are used to charge the battery pack.

Boost PFC three-phase configuration (Figure 1.4) permits a higher power flow and a better harmonics quality in the reverted electrical quantity on the DC side.

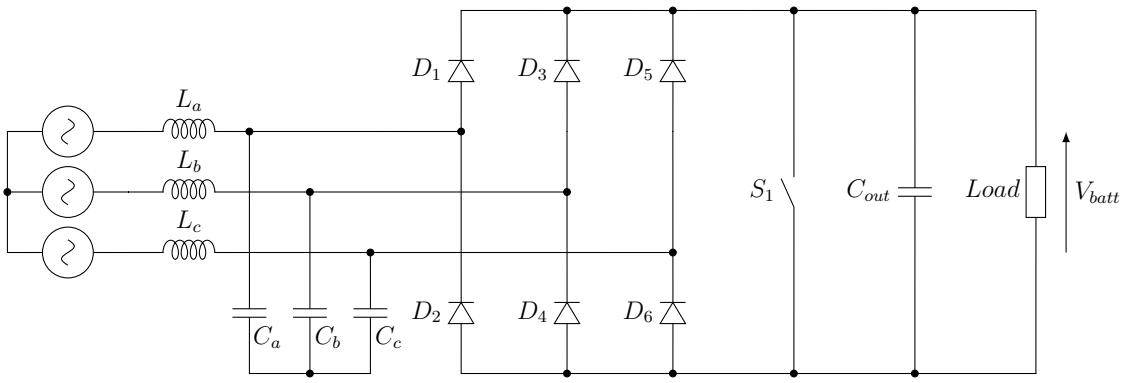

Figure 1.4: Three-phase boost PFC

A even better solution in terms of harmonic distortion is the t-type converter (Figure 1.5, [5]). Unlike the previous configuration that is a two-levels converter, the T-type converter is a three-levels converter and it permits to increase the available instant values of the voltage by one. The use of the T-type converter leads to some advantages:

- better accuracy in the regulation
- lower harmonic content of the electrical quantities
- smaller filter components, due to the lower harmonics content of the electrical quantities
- low switch voltage stress
- lower switching loss

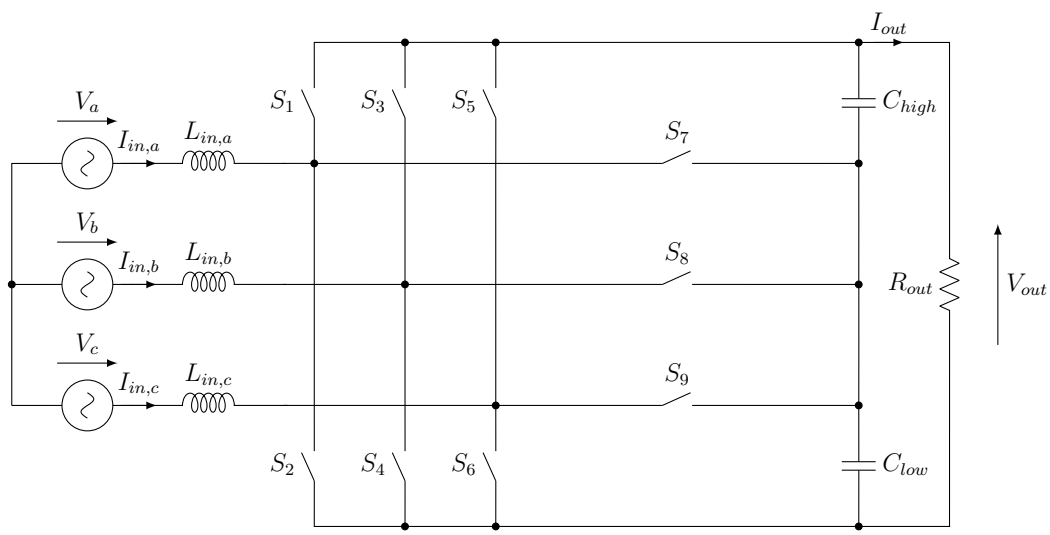

Figure 1.5: Three-phase T-type converter

In the case of this project, another advantage is given by the T-type structure itself. In fact it can be used both in three-phase supply systems (one voltage source for each phase) and single-phase supply systems (one single voltage source for all converter phases in a parallel configuration).

The disadvantages of the T-type converter that could be mentioned are the higher number of switches needed and the control complexity. Moreover, this topology requires higher DC-link voltage if compared with simpler solutions.

In order to reduce weight and volume of the converter, and at the meantime guaranteeing galvanic isolation of the battery, in automotive application a HF DC/DC converter is mostly used, so the galvanic isolation is given by a smaller transformer

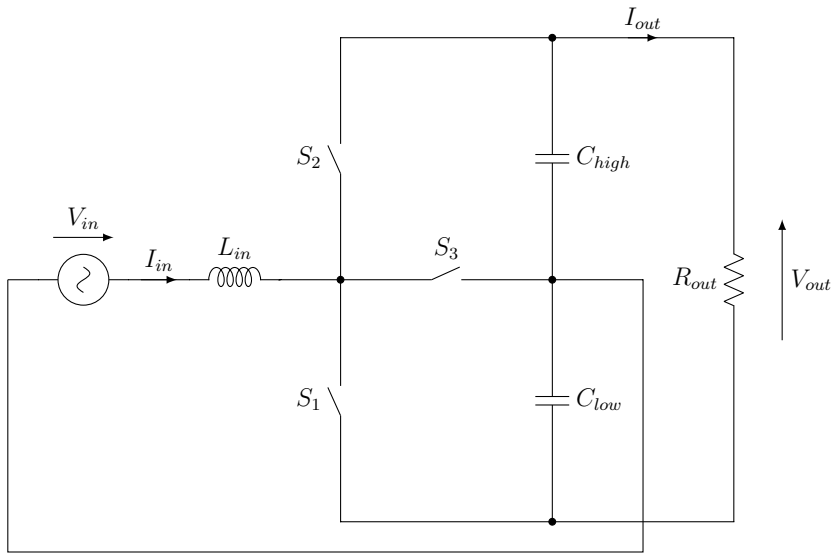

Figure 1.6: Single-phase T-type converter

if compared with a LF one. Nowadays two of the most common isolated DC/DC converters adopted in automotive are the LLC and phase shifted (PS) converter.

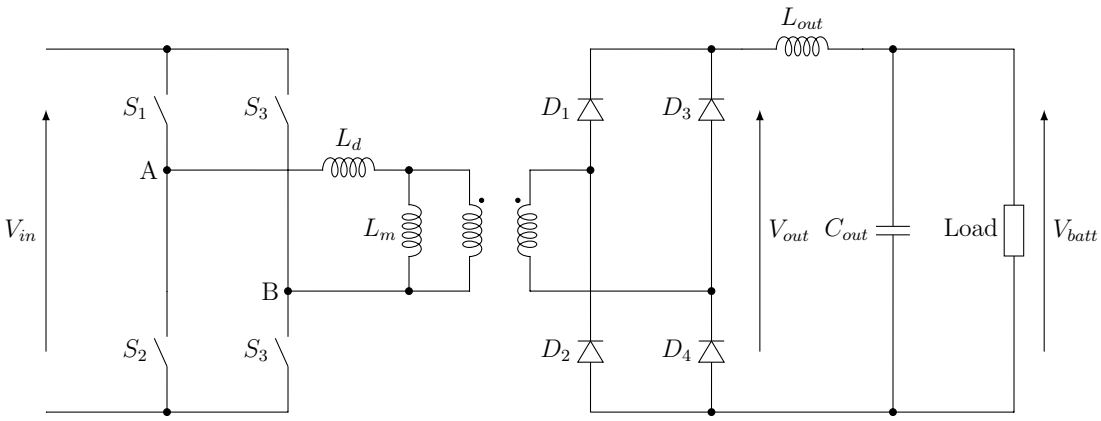

Figure 1.7: Phase-shifted full bridge converter

The phase-shifted converter (Figure 1.7,[6]) is composed of an active full bridge that works at constant frequency, a HF transformer and a diode rectifier at the output stage. The output voltage is regulated by shifting the phases of gate pulses of the lagging and leading legs. A very useful advantage of this converter is the Zero Voltage Switching (ZVS) during the active switches turn-off, that improve the

efficiency of the global battery charger. In fact, common DC/DC converters the parasitic elements, such as parasitic capacitances, are unwanted elements, however the phase-shifted converter use this capacitance to let the switches turn-off with a zero voltage applied to their terminals. To guarantee the ZVS, the energy stored in the inductances must be high enough to charge and discharge the parasitic capacitance. This lead to understand that for light loads the ZVS may not occur.

Another DC/DC converter that can be used is the LLC converter (Figure 1.8, [7]). Its configuration is very similar to the phase-shifted one, however LLC converter presents a resonant tank after the active bridge and the output voltage is regulated by controlling the frequency of the electrical quantities that flow through the transformer. This configuration gives many advantages:

- small current ripple at output stage
- small size of components if well designed (resonant tank can be part of the transformer, saving weight and volume)
- ZVS in a wide range of load levels
- very high efficiency

The worst drawbacks are the control complexity and the difficulty in finding the right reactive component in order to set up the resonant tank and the transformer, in fact in most cases, this components are custom made.

1.4 Specifications of the project

The project developed in this work is part of FITGEN (Functionally Integrated e-axle ready for mass market Third GENeration electric vehicles) project, founded by European Unions H2020 research and innovation programme under Grant Agreement no. 824335. FITGEN aims to develop a brand-independent fully electric vehicle architecture and it is divided into three different areas:

1. *Power electronics and charger*
2. *Electric motor and transmission*

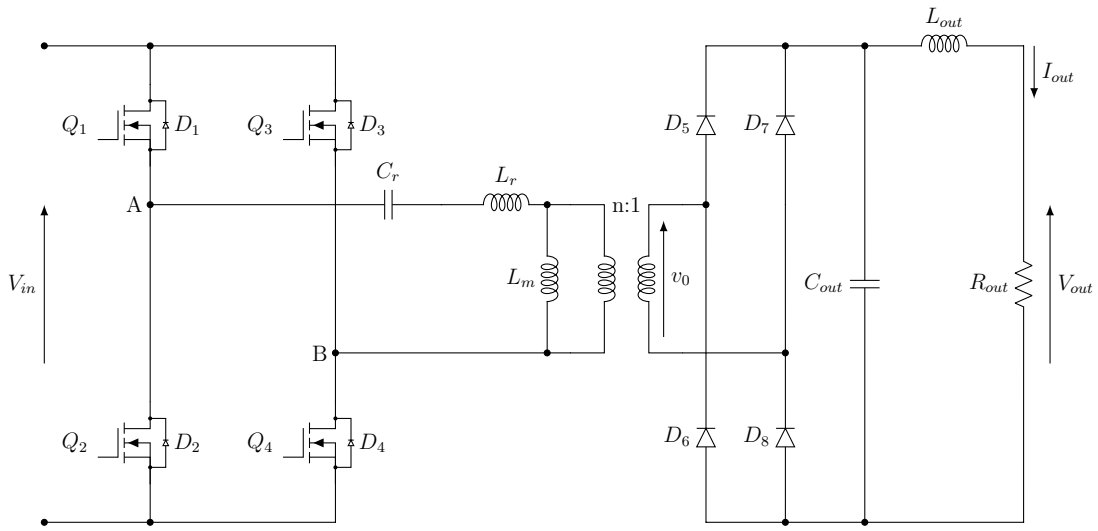

Figure 1.8: LLC converter

3. *Cooling and control*

The areas of FITGEN cover all the technical challenges with innovative and highly integrated solutions.

Among the other goals of the project, it is required to develop an OBC with high power density and high efficiency. The desired charging profile (Figure 1.9) is divided in two intervals. In the first part of the recharging process the current in constant and kept to its nominal value. The battery voltage is low and it increases with time. When the voltage reaches its maximum value it remains constant and the current starts to decrease, reaching values close to zero. The working point in which the current starts to decrease represents the transition between the first and the second interval of the charging profile. The recharging process stops when the current becomes lower than a threshold value, which is close to zero. The control system must ensure that the electrical quantities, such as current and voltage, on the battery side will follow the trend lines described by the charging profile.

In order to obtain high efficiency and low power losses, Silicon-Carbide (SiC) component are used for inverters and rectifiers in the battery charger. The provider of Mosfets and diodes is STMicroelectronics.

Another specification given by FITGEN is to obtain a flexible OBC, which can

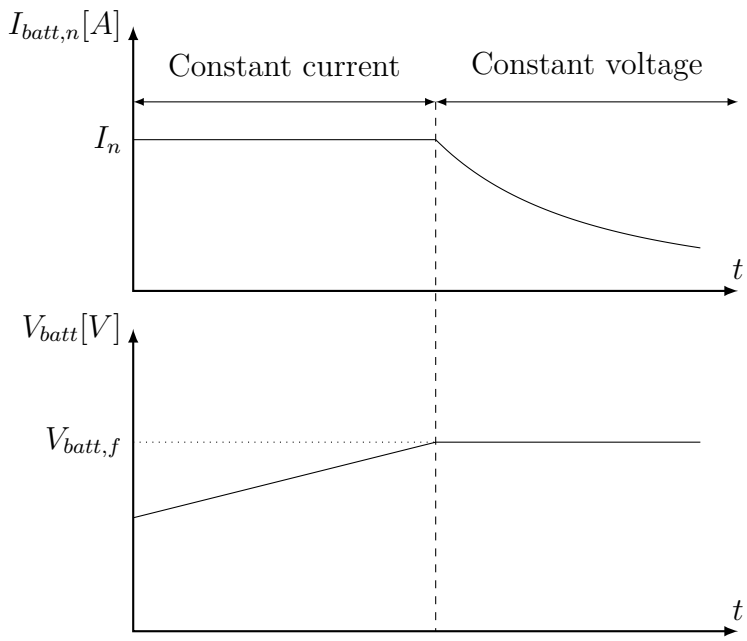

Figure 1.9: Charging profile of an EV battery pack

be used both in single- and three-phase configurations. The rated power are respectively 6kW and 11kW. Another interesting feature of the FITGEN e-axle is the affordable integrated fast-charging capability through an external charger (up to 750V, 120kW peak). Anyway, this topic will not be covered by this thesis.

1.5 Proposed solution

The proposed solution is composed of a three-phase T-type converter as AC/DC stage and a LLC Converter as DC/DC converter.

The choice of the T-type converter for the AC/DC stage is justified by adaptation requirements. Despite the possible difficulties in terms of power control, the specifications imposed by the FITGEN project do not include V2G charger so the input rectification is made by a diode bridge. In this way the control, as described in details in a dedicated chapter of this work, can be compared to the control of a simple single-phase boost converter. Moreover, as the improvement of the harmonics quality of the electrical quantities leads to a smaller reactive components, the choice of the T-type converter is a good solution in an automotive environment,

where weight and volumes are critical issues, although the higher switches number if compared with simpler configurations.

LLC converter is chosen because it leads to a higher efficiency and the ZVS can be ensured in a wide range of power level, improving the adaptation of the global battery charger.

Chapter 2

Analysis of the proposed structure

As the battery charger is composed of two cascaded power converters, in this chapter both of them are introduced and analyzed to illustrate their working principles and their control strategies. The goal here is to understand how the T-type converter and the LLC converter work individually and, finally, how they are working together forming the complete battery charger.

2.1 The unidirectional T-type converter

Analyzing the power flow from the grid to the battery pack, the first converter that is found is the T-type converter, which can assume both the single-phase and three-phase configurations (Figure 2.1).

Regardless of the configuration, the task of the T-type converter is to rectify the AC grid voltage to a DC form in the DC-link, while maintaining a unitary power factor seen from the grid. In this way it is possible to reduce harmonic distortion and its associated losses, improving the power quality at the battery charger input.

The proposed T-type structures are unidirectional in terms of power flow, so there are ideally just three active switches (S_1, S_8, S_9) in the three-phase configuration and one active switch (S_3) in the single-phase configuration. All the others switch are freewheeling diodes. simplifies the converter control strategy and

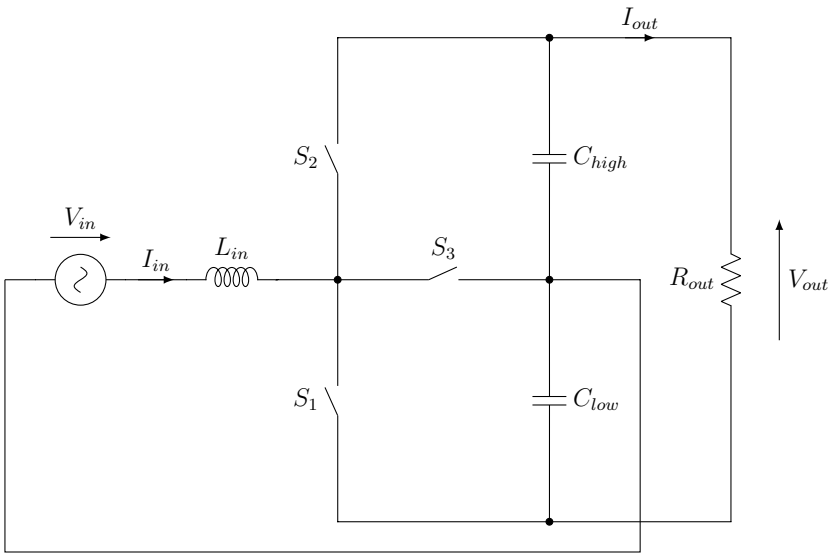

(a) Single-phase configuration

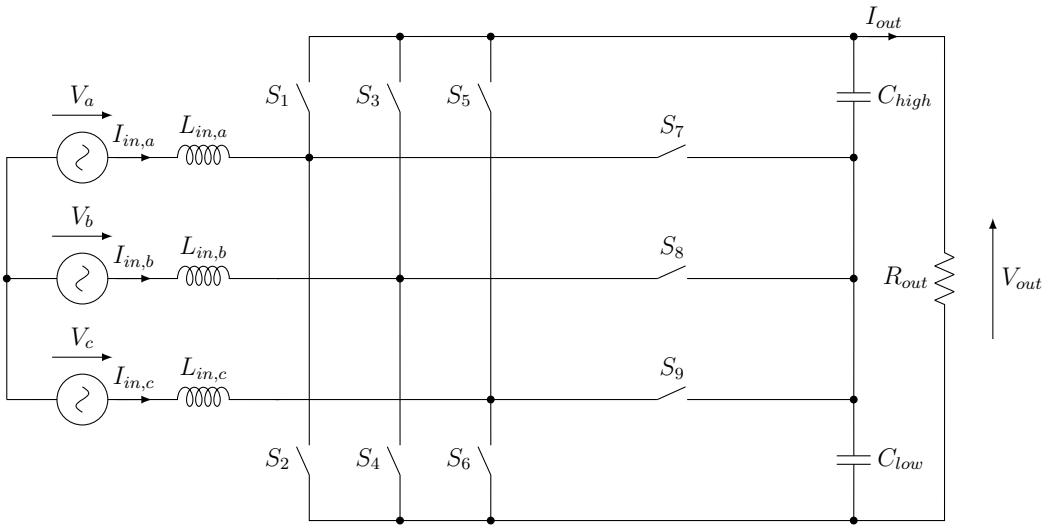

(b) Three-phase confuguration

Figure 2.1: T-type converter circuit scheme

reduces the number of components used for the control circuit. In fact, in bidirectional structures, diodes are replaced by active switches (Figure 2.2) giving a leg structure that requires more complicated control strategies, like 3-level Space Vector Modulation [8], and more driver circuit designed for high frequency. So, in the proposed structure, one leg of the rectifier presents two diodes and ideally one

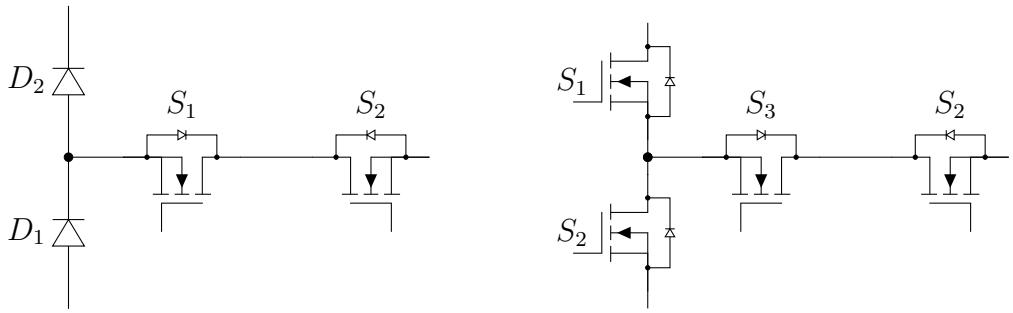

(a) Unidirectional (b) Bidirectional

Figure 2.2: T-type leg structures

active switch, which in the real application is composed of two power MOSFETs driven by the same gate signal.

Besides the switches, there are also three input inductors (one per phase) that are used as current filters and two output capacitors used to filter the DC-link voltage V_{DC}. These two capacitors are identical, so the DC-link voltage is, in principle, divided into two equal parts on the two capacitors.

Depending on the configuration of the converter (single-phase or three-phase), two different control strategies are adopted that are described in the next paragraphs.

Finally, as in the control scheme the input voltage value is required, a Phase Locked Loop (PLL) must be implemented, both for single-phase and three-phase configurations.

2.1.1 Single-phase T-type converter

Driving the active switch (S_3 in the single-phase configuration) it is possible to regulate the voltage on the input inductor and consequently the current that flows through it. The voltage v_L applied to the input inductor can assume different values depending on the input current direction and the gate signal $s_x(t)$ of the active switches ($s(t) = 1$ for closed active switches, $s(t) = 0$ for opened active

switches):

$$i_{in}(t) \geq 0 \Rightarrow v_{Lx}(t) = \begin{cases} v_{in} & \text{when } s_x(t) = 1 \\ v_{in} - \dfrac{V_{dc}}{2} & \text{when } s_x(t) = 0 \end{cases} \tag{2.1}$$

$$i_{in}(t) \leq 0 \Rightarrow v_{Lx}(t) = \begin{cases} v_{in} & \text{when } s_x(t) = 1 \\ v_{in} + \dfrac{V_{dc}}{2} & \text{when } s_x(t) = 0 \end{cases} \tag{2.2}$$

It is important to note that during one half of the current period just two voltage values of $v_L(t)$ are available so the complete structure behaves like two cascaded boost converters that work alternatively at each half waveform of the input current (Figure 2.3). This fact dictates an important restriction to be considered when designing the converter: the voltage applied to a single output capacitor must be higher than the input voltage peak value or, in other words, the DC-link voltage must be higher than the peak-to-peak input voltage.

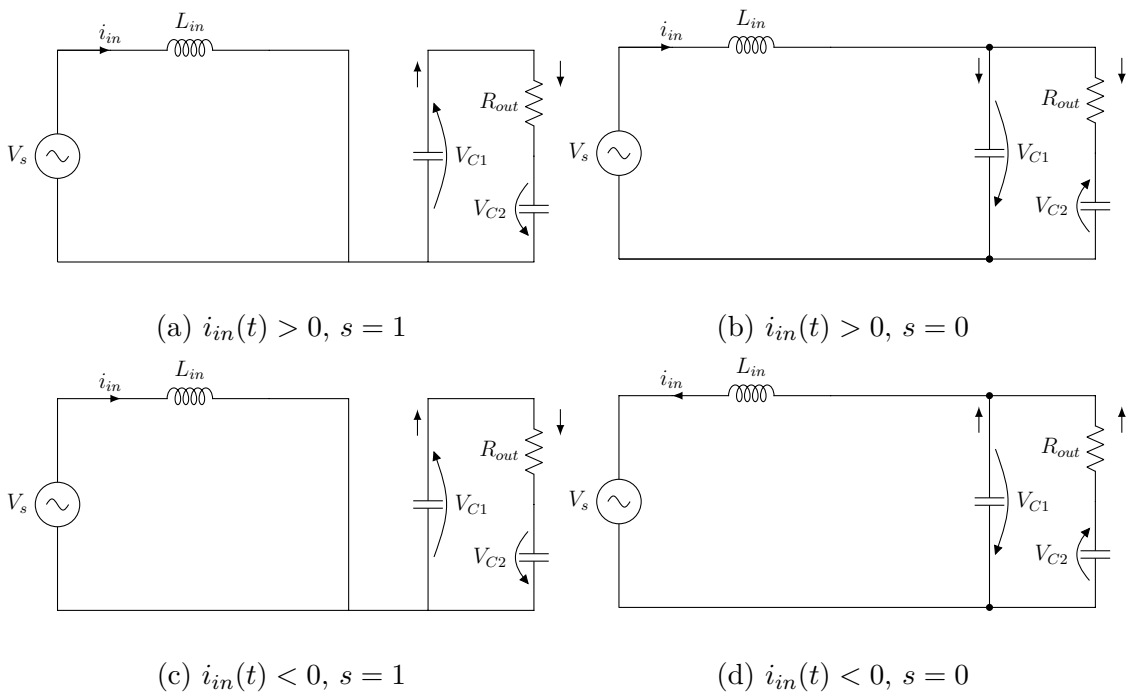

(a) $i_{in}(t) > 0$, $s = 1$ (b) $i_{in}(t) > 0$, $s = 0$

(c) $i_{in}(t) < 0$, $s = 1$ (d) $i_{in}(t) < 0$, $s = 0$

Figure 2.3: T-type equivalent circuits depending on current direction and gate signal

Since the rectifier has to work as a PFC, guaranteeing a high power factor on the grid side, the grid voltage and current should always have the same sign. So, when the input voltage is positive the input current should be positive as well and if the active switch is closed a positive voltage is applied to the input inductor and the current that flows through it tends to increase. Vice versa, if the active switch is closed a negative voltage is applied to the inductor and the current tends to decrease.
Analyzing the situation with a negative input voltage (so the input current is negative too), it could be found that the current behaves in a similar manner, with opposite sign. In both cases, when the active switch is closed the input current tends to increase in magnitude and when the active switch is open the current tends to decrease.

2.1.2 Cascaded current and voltage control loops

Normally, the T-type converter is controlled by two control loops (Figure 2.4). A inner current loop is used to drive the active switches in such a way that the input current results in phase with the input voltage, giving a unitary power factor (Figure 2.5) and the outer voltage loop impose the DC-link voltage value.

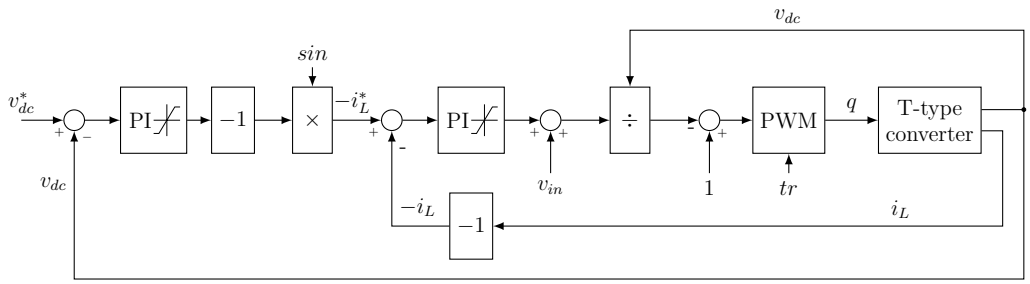

Figure 2.4: Control scheme of the single-phase T-type converter

The input of the control scheme is the desired DC-link voltage and the comparison with the measured value is sent to a PI regulator. Its output correspond to the magnitude of the desired input current. As the input current bust be sinusoidal, the output of the PI regulator is multiply by a unitary sine wave which is in phases

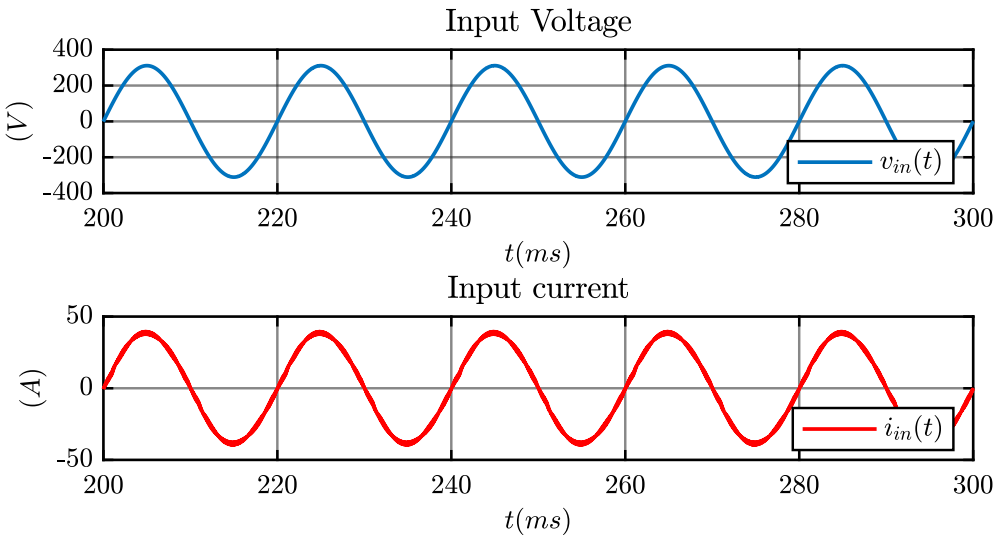

Figure 2.5: Typical input voltage and current waveforms for a PFC converter

with the input voltage. In this way, the reference signal of the current loop is constructed. The difference between this signal and the measured input current is sent to the PI regulator of the current control loop.

A feed-forward signal, equal to the measured input voltage, is then added to the output of the current regulator. The result is then divided by the voltage applied to the output capacitor and subtracted to 1, obtaining the required duty cycle. The gate signal q is generated using the PWM technique in which the duty cycle d is compared with a triangular wave that vary from 0 to 1. In order to use the same control scheme for both the situation with positive and negative input voltage, it is enough to change the construction of the signal v^* depending on the input voltage polarity:

$$v_{in}(t) \geq 0 \;\Rightarrow v^* = v^*_{Lin} + v_{in} \tag{2.3}$$

$$v_{in}(t) < 0 \;\Rightarrow v^* = -v^*_{Lin} - v_{in} \tag{2.4}$$

With this construction the duty cycle d can always be compared with the triangular wave in the right way. Furthermore, the signal v_{out} used to construct the duty cycle does not correspond to the output voltage of the T-type converter (the

DC-link voltage) but it corresponds to the output voltage of the boost converter structures. Consequently, v_{out} is equal to $v_{c,high}$ when the input current is positive and to $v_{c,low}$ when the input current is negative.

The parameters $k_{p,i}$ and $k_{i,i}$ of the current PI can be set as following:

$$\omega_i = 2 \cdot \pi \cdot f_s \cdot 0.05 \tag{2.5}$$

$$k_{p,i} = \omega_i \cdot L_{in} \tag{2.6}$$

$$k_{i,i} = 0.1 \cdot \omega_i \cdot k_{p,i} \tag{2.7}$$

where:

- $fs[Hz]$: is the switching frequency
- $\omega_i[rad/s]$: is the current loop bandwidth, which is set to a value that corresponds to one tenth of the switching frequency
- $L_{in}[H]$: is the input inductance value

The parameters of the voltage PI are tuned as follow:

$$\omega_v = 0.01 \cdot \omega_i \tag{2.8}$$

$$k_{p,v} = \omega_v \cdot C_{out} \tag{2.9}$$

$$k_{i,v} = 0.01 \cdot \omega_v \cdot k_{p,v} \tag{2.10}$$

where:

- $\omega_v[rad/s]$: is the voltage loop bandwidth, which is set to a value that corresponds to one tenth of the current loop bandwidth
- $C_{out}[F]$: is the capacitance value of the output capacitors

The voltage loop bandwidth is set to a value that is less than the input frequency so the current reference signals can assume a more sinusoidal waveform. In fact, in this kind of application precision is more important than response time.

2.1.3 The Discontinuous Conduction Mode

As the current is controlled in order to assume a sinusoidal form, in the first and last instants of a half period of the fundamental frequency the Discontinuous Conduction Mode (DCM) may happen so the sampled current value does not correspond to the actual mean current value and could not be controlled in a right way. The DCM can occur when the current ripple is higher than the mean current. This can happen either for low average phase current or for high ripple systems (Figure 2.6).

During the DCM, the sampled current value must be corrected through the introduction of a corrective coefficient k_{corr} [9]:

$$k_{corr} = d \cdot \frac{v_{out}}{v_{out} - v_{in}} \tag{2.11}$$

The DCM must be taken into account also in the current control loop modifying the construction of the signal v^*:

$$v_{in}(t) \geq 0 \;\Rightarrow v^* = v^*_{Lin} + v_{in} + (1 - k_{corr}) \cdot (v_{out} - v_{in}) \tag{2.12}$$

$$v_{in}(t) < 0 \;\Rightarrow v^* = -v^*_{Lin} - v_{in} + (1 - k_{corr}) \cdot ((v_{out}) - v_{in}) \tag{2.13}$$

2.1.4 Interleaved single-phase T-type converter and current control with phase interleaving

Taking advantage of the three-phase input T-type power modules, the single-phase structure can become a single-phase inlet, three-leg interleaved T-type converter

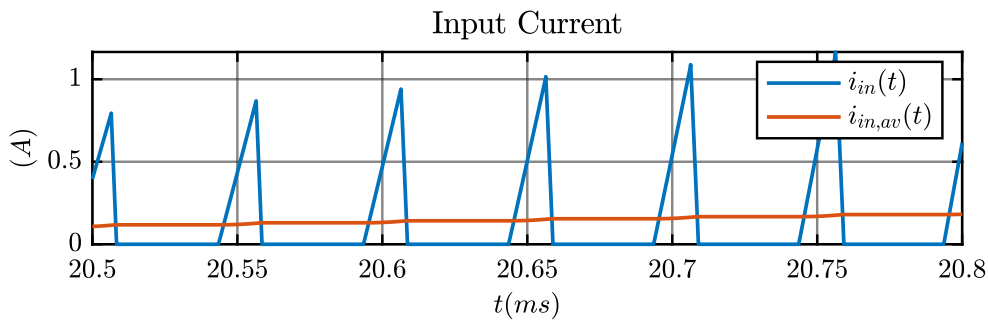

Figure 2.6: Current waveform in Discontinuous Conducting Mode (DCM)

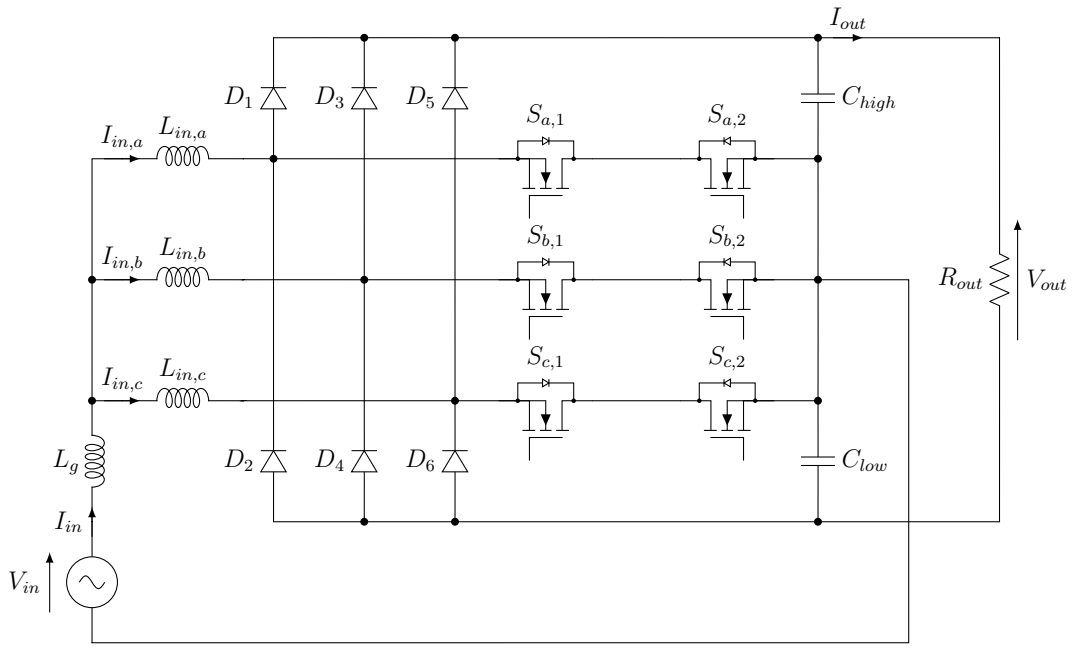

Figure 2.7: Proposed structure for the single-phase T-type converter

(Figure 2.7). This structure introduces many advantages:

- adaptation of the converter to both single-phase and three-phase supply system
- lower current that flows through the inductors
- inductors of smaller size, dictated by the specs of the three-phase solution. A single leg single-phase inlet T-type converter would require an inductor of triple size, current wise

The interleaving technique consists in delaying in time the gate signals one from another by one third of the switching period (Figure 2.8). The instantaneous phase currents assume different values from each other, but the average value is the same for all of them.

For equal input inductance and switching frequency, the interleaving technique leads to a smaller ripple of the input current, so it is possible to satisfy the standards requirements with smaller input inductors. The converter is also improved in terms of weight and volume. Due to this consideration, the interleaving technique is adopted for this work.

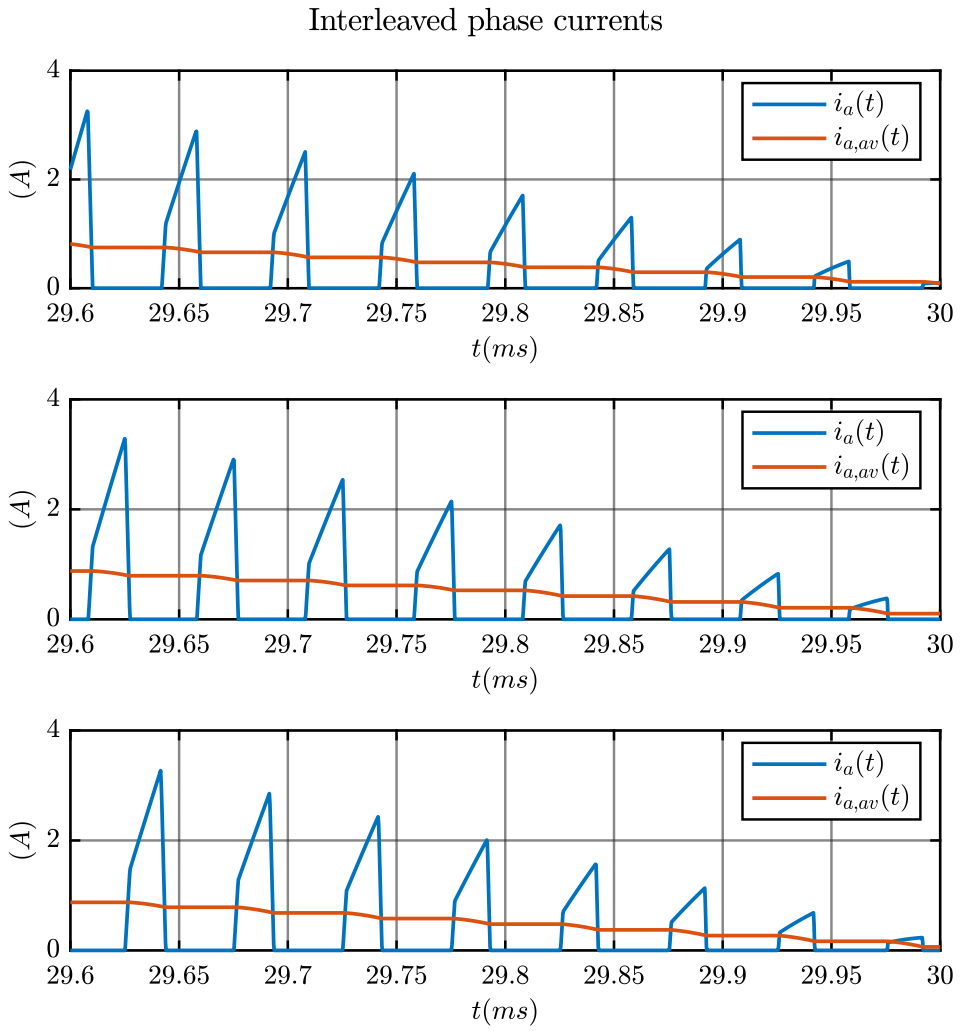

Figure 2.8: Phase currents waveforms with interleaved gate signals

Due to the interleaving technique, three current loops are required, one for each phase of the converter. Each current control loop works in the same way as described in Figure 2.4 and their PI regulators are tuned in the same way. The only difference in this case is caused by a different reference current. In fact, in this T-type structure it is possible to control the current flowing through the inductors. Consequently, the output of the voltage loop, which determines the desired input current, must be divided by three in order to construct the input signals of the

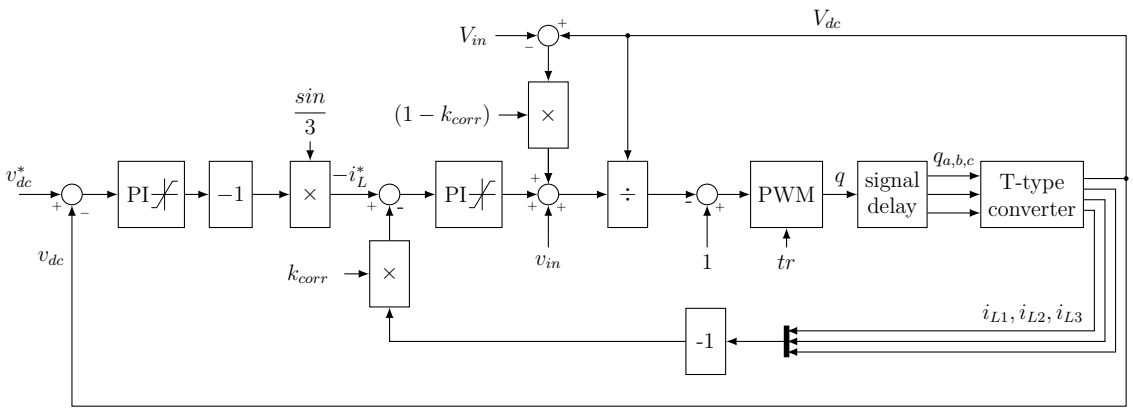

Figure 2.9: Complete control scheme of the single-phase T-type converter

currents control loops.

Considering the DCM and the interleaving technique, the control scheme reported in Figure 2.4 must be modified. The control scheme used in this work is reported in Figure 2.9. It is possible to note that the measured currents are multiplied for the correction factor k_{corr} and then compared with the reference current i^*_L, which is the same for all the three PI regulators. Note that in Figure 2.9 the current PI block represents in reality all the three current PI regulators. The signal used to construct the duty cycles is modified because of DCM. Finally, the gate signals are delayed each other before to be sent to the T-type converter. The voltage loop works in the same way as described before.

2.1.5 Control strategy for unidirectional three-phase T-type converter

Also for the three-phase T-type converter (Figure 2.10) the control is composed of a inner current loop and an outer voltage loop (Figure 2.11).

First of all, the reference DC-link voltage value is compared with its actual value and the difference is set to the PI regulator of the voltage loop. The current control is implemented in dq coordinate, where the position of the d-axis is imposed by the phase of the grid voltage. The output of the voltage loop sets the reference i^*_d, while i^*_q is set to zero for the sake of having grid current in phase with the grid

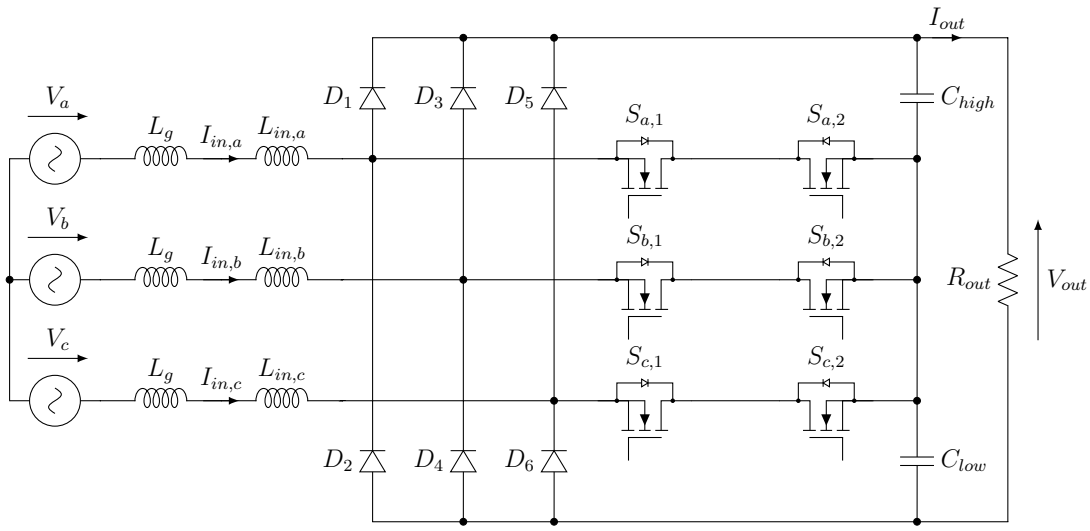

Figure 2.10: Proposed structure for the three-phase T-type converter

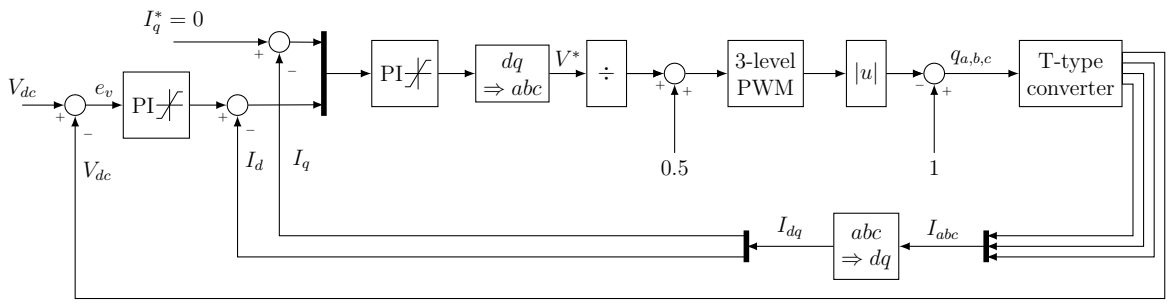

Figure 2.11: Control scheme for the three-phase T-type converter

voltage, and so obtaining unitary power factor.

The reference current values must be compared with the actual values, so the measured 3-phase currents are transformed into dq components by using Clarke

and Park transformations:

$$\begin{bmatrix} u_\alpha \\ u_\beta \\ u_0 \end{bmatrix} = \begin{bmatrix} \frac{2}{3} & -\frac{1}{3} & -\frac{1}{3} \\ 0 & \frac{1}{\sqrt{3}} & \frac{1}{\sqrt{3}} \\ \frac{1}{3} & \frac{1}{3} & \frac{1}{3} \end{bmatrix} \begin{bmatrix} u_a \\ u_b \\ u_c \end{bmatrix} \tag{2.14}$$

$$\begin{bmatrix} u_d \\ u_q \\ u_0 \end{bmatrix} = \begin{bmatrix} cos(\omega t) & sin(\omega t) & 0 \\ -sin(\omega t) & cos(\omega t) & 0 \\ 0 & 0 & 1 \end{bmatrix} \begin{bmatrix} u_\alpha \\ u_\beta \\ u_0 \end{bmatrix} \tag{2.15}$$

Of course, the homopolar component is not used in the control scheme.

The difference between desired and measured dq current components is sent to the PI regulators of the current loop. Its output is composed of the required voltage in dq coordinates so, before to be compared with the triangular wave of the PWM modulation, they are reported in abc coordinates using the inverse transformations:

$$\begin{bmatrix} u_\alpha \\ u_\beta \\ u_0 \end{bmatrix} = \begin{bmatrix} cos(\omega t) & -sin(\omega t) & 0 \\ sin(\omega t) & cos(\omega t) & 0 \\ 0 & 0 & 1 \end{bmatrix} \begin{bmatrix} u_a \\ u_b \\ u_c \end{bmatrix} \tag{2.16}$$

$$\begin{bmatrix} u_a \\ u_b \\ u_c \end{bmatrix} = \begin{bmatrix} 1 & 0 & 1 \\ -\frac{1}{2} & \frac{\sqrt{3}}{2} & 1 \\ -\frac{1}{2} & -\frac{\sqrt{3}}{2} & 1 \end{bmatrix} \begin{bmatrix} u_\alpha \\ u_\beta \\ u_0 \end{bmatrix} \tag{2.17}$$

The modulating signal is created dividing the output of the current regulator by the DC-link voltage value. The modulation uses a Three-level PWM, which output signals can be either -1, 0 or 1 and they normally correspond to three different voltage levels. However, the only active switches that can be driven are the middle ones so the gate signals must be modified.

In the proposed structure the modulating signals $v_{xm}*$ tend to increase in amplitude when the current error e_i tends to increase too. Consequently, if the output

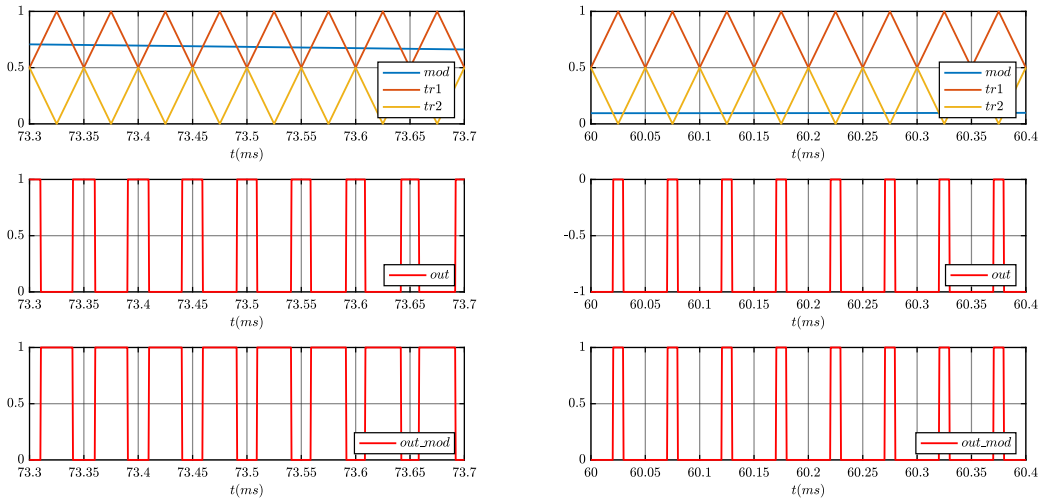

(a) $v_x^*(t) > 0$ (b) $v_x^*(t) < 0$

Figure 2.12: Three-level PWM: triangular carriers, modulating signal, non-modified and modified outputs

signals of the PWM were directly used to drive the active switches without being modified they would create a voltage value v_{xm} that decreases the phase current. Therefore, the control would try to increase the current amplitude, but the actuator tends to decrease it.

Due to the above consideration, the PWM output signals are modified in such a way that when the control want to increase the input current amplitude, the duty cycle of the middle active switch is increased (Figure 2.12).

The PI regulators are tuned in the same way as for the single-phase configuration ((2.5) to (2.7) and (2.8) to (2.10)).

2.1.6 PLL scheme for single-phase T-type converter

The control scheme of the T-type converter requires to retrive of the input voltage sine waveform in both single-phase and three-phase configurations. In the single-phase configuration the signal is used to form the current loop input and in the three-phase configuration it is used for Clarke and Park transformations. The reconstruction of the input voltage signal is made by a Phase Locked Loop (PLL),

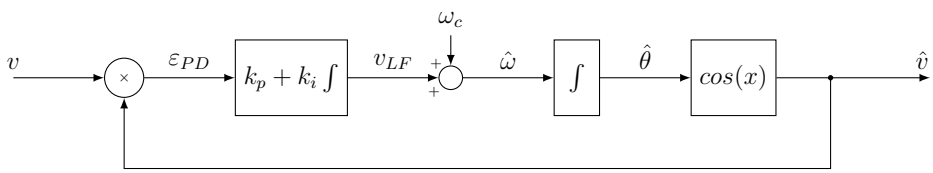

Figure 2.13: PLL scheme for single-phase T-type converter

which is composed of a closed loop system that keeps the time of some external periodical signal using the feedback loop. The scheme of the PLL is different depending on the system configuration.

The PLL scheme for single-phase systems (Figure 2.13) is composed of three fundamental blocks [10]:

- *Phase Detector (PD)*: this block generates an output ε_{PD} that is proportional to the phase difference between the input signal and the signal generated by an internal oscillator

- *Loop Filter (LF)*: this block is a low-pass filter used to reduce the high frequency components of the signal generated by the PD and in this work it is constituded by a PI controller

- *Voltage-Controlled Oscillator (VCO)*: this block generates a signal that is phase shifted with respect to a given central frequency ω_c and that depends on the signal v_{LF} provided by the LF block

The input signal applied to the PLL is the input measured voltage:

$$v = V sin(\theta) = V sin(\omega t + \phi) \tag{2.18}$$

and the output signal generated by the VCO block is given by:

$$v' = cos(\hat{\theta}) = cos(\hat{\omega} + \hat{\phi}) \tag{2.19}$$

The phase error at the PD block output can be calculated as follow:

$$\begin{aligned}\epsilon_{PD} &= V sin(\omega t + \phi) cos(\hat{\omega} t + \hat{\phi}) \\ &= \frac{V}{2}\Big[sin\big((\omega - \hat{\omega})t + (\phi - \hat{\phi})\big) + sin\big((\omega + \hat{\omega})t + (\phi + \hat{\phi})\big)\Big]\end{aligned} \tag{2.20}$$

The second term between parenthesis represents the high frequency component of the PD output signal and it is attenuate by the PI regulator so it is possible to consider just the low frequency term of the signal. In this way it is possible to consider the ε_{PD} signal as follow:

$$\bar{\varepsilon}_{PD} = \frac{V}{2} sin\big((\omega - \hat{\omega})t + (\phi - \hat{\phi})\big) \tag{2.21}$$

Assuming that the PLL is well tuned, the frequency at the output of the oscillator is very closed to the frequency of the input signal ($\hat{\omega} \approx \omega$) it is possible to further simplify the phase error signal:

$$\bar{\varepsilon}_{PD} = \frac{V}{2} sin(\phi - \hat{\phi}) \tag{2.22}$$

When the phase error is very small it is possible to linearize (2.22):

$$\bar{\varepsilon}_{PD} = \frac{V}{2}(\phi - \hat{\phi}) \tag{2.23}$$

The average frequency of is given by:

$$\hat{\bar{\omega}} = \omega_c + \bar{v}_{LF} \tag{2.24}$$

while the small signal variation is given by:

$$\tilde{\hat{\omega}} = \tilde{v}_{LF} \tag{2.25}$$

Finally, the variations in the phase-angle detected by the PLL can be calculated

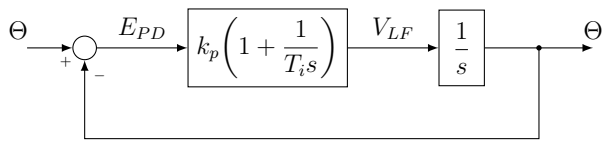

Figure 2.14: Small signal model of PLL for single-phase T-type converter

by:

$$\tilde{\hat{\phi}}(t) = \int \tilde{\hat{\omega}} dt = \int \tilde{v}_{LF} dt \tag{2.26}$$

With these equations it is possible to construct the small signal model of PLL in Laplace domain (Figure 2.14). The closed loop transfer function in the normalized form is given by:

$$H_\phi(s) = \frac{2\zeta\omega_n s + \omega_n^2}{s^2 + 2\zeta\omega_n s + \omega_n^2} \tag{2.27}$$

where:

$$\omega_n = \sqrt{\frac{k_p}{T_i}} \qquad \zeta = \frac{\sqrt{k_p T_i}}{2}$$

As 2.27 represents a second order transfer function, the settling time t_s responding to a step input can be approximated by:

$$t_s = 4.6\tau \tag{2.28}$$

where:

$$\tau = \frac{1}{\zeta\omega_n} \tag{2.29}$$

These expressions can be used to tune the PI controller:

$$k_p = 2\zeta\omega_n = \frac{9.2}{t_s} \tag{2.30}$$

$$T_i = \frac{2\zeta}{\omega_n} = \frac{t_s\zeta^2}{2.3} \tag{2.31}$$

If the amplitude input voltage is different from 1, the parameters in 2.31 must be divided by the actual input voltage amplitude V. Furthermore, it is worth to remember that these expressions are just a guide to tune the PI controller and they can be modified in order to obtain better parameters values.

2.1.7 PLL scheme for three-phase T-type converter

The PLL scheme adopted for the three-phase configuration (Figure 2.15) is not so different from the previous one.

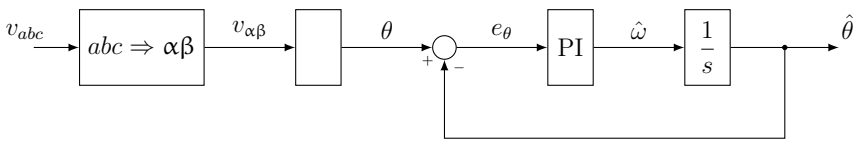

Figure 2.15: PLL scheme for three-phase T-type converter

In this configuration, the input of the PLL is composed of the measured input voltages v_{abc} which are transformed using Clarke transformation to obtain the components $v_{\alpha\beta}$. The components referred to the $\alpha\beta$ coordinate system are used to computed the phase angle θ (Figure 2.16).

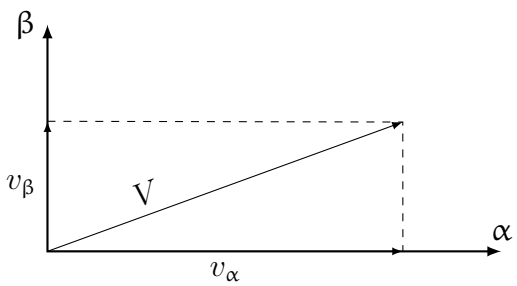

Figure 2.16: Representation of the voltage space vector in $\alpha\beta$ coordinates system

So, starting from $v_{\alpha\beta}$ it is possible to write:

$$V = \sqrt{v_\alpha^2 + v_\beta^2} \tag{2.32}$$

$$\cos\theta = \frac{v_\alpha}{V} \tag{2.33}$$

$$\sin\theta = \frac{v_\beta}{V} \tag{2.34}$$

Assuming that the PLL is well tuned, the difference between real and estimated voltage angle ($\theta - \hat{theta}$) is very small. So the phase angle error e_θ can be calculated by using:

$$e_\theta = \theta - \hat{\theta} \approx sin(\theta - \hat{\theta}) = sin\theta cos\hat{\theta} - cos\theta sin\hat{\theta} \tag{2.35}$$

(2.35) permit to avoid the discontinuities due tho the value of the voltage angle, which vary from 0 to 2π. The error e_θ is sent to a PI regulator which parameters are set as follow:

$$\omega_{PLL} = 2 \cdot \pi \cdot f_s \cdot 0.1 \tag{2.36}$$

$$k_{p,PLL} = \omega_{PLL} \tag{2.37}$$

$$k_{i,PLL} = k_{p,PLL} \cdot 0.1; \tag{2.38}$$

The output of the PI regulator is adopted as estimated pulsation $\hat{\omega}$. This signal is integrated to obtain the estimated phase angle $\hat{\theta}$ and its components $cos\hat{\theta}$ and $sin\hat{\theta}$, used as feedback. Once obtained $cos\theta'$ and $sin\theta'$, these components are used for the Park transformations in the three-phase T-type control scheme.

2.2 LLC converter

The LLC converter (Figure 2.17) is a DC/DC converter which functioning is based on the resonant interaction between the reactive components of the resonant tank.

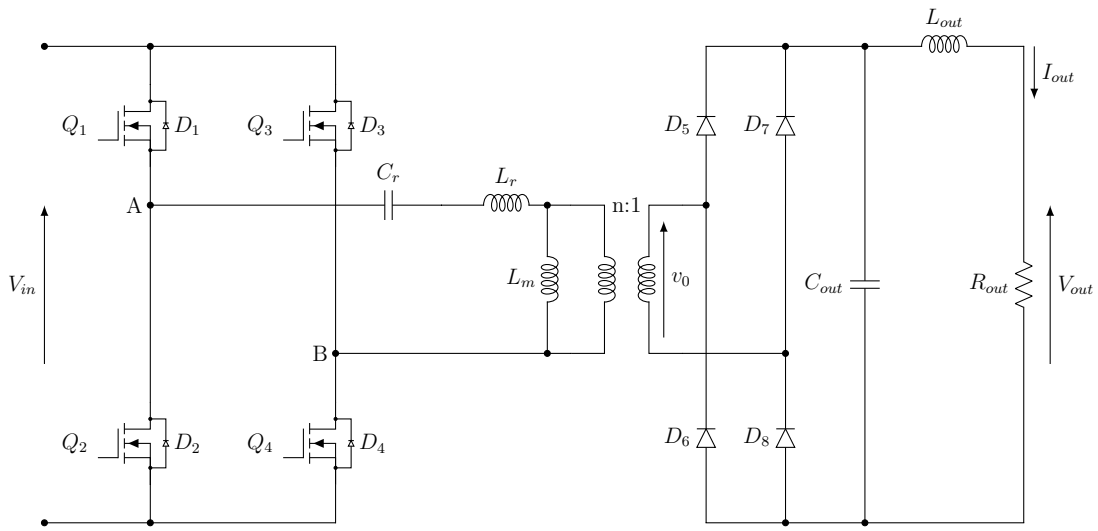

Figure 2.17: LLC converter

The bridge inverter is controlled with a constant duty cycle $d = 0.5$, so the voltage at the resonant tank terminals has a square waveform with magnitude equal to $V_{dc}/2$ and variable frequency.

2.2.1 First Harmonic Approximation

A good way to understand the working principle of the LLC converter is to use the First Harmonic Approximation (FHA) which gives a easy procedure and an easy model that represent the complete converter.

First of all, the FHA consider just the fundamental of the input square wave, so it is possible to assume that the resonant tank is supplied by an AC sinusoidal voltage source which amplitude is equal to:

$$V = \frac{2}{\pi} V_{DC} \tag{2.39}$$

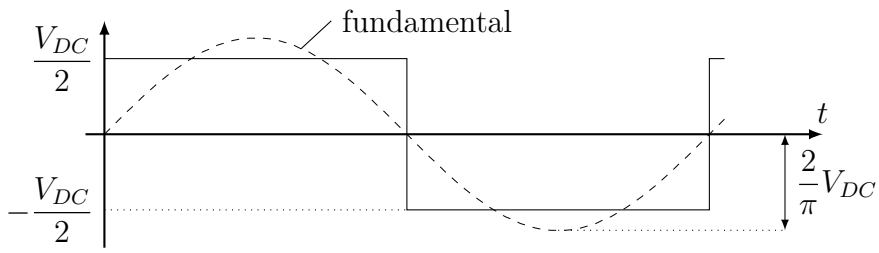

Figure 2.18: Representation of a square wave and its fundamental component

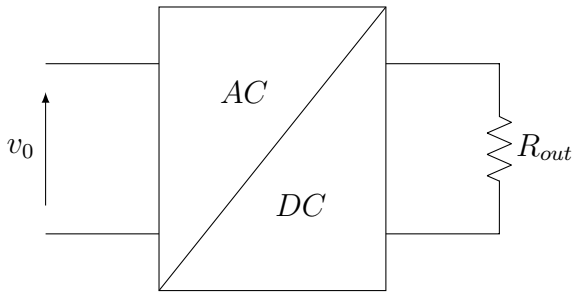

Figure 2.19: Load model

where V_{DC} is the value of the DC-link voltage. V represent the amplitude of the fundamental harmonic component of a square wave that vary from $-V_{DC}/2$ and $+V_{DC}/2$ (Figure 2.18). The rms value of the voltage source is then given by:

$$V_{in,rms} = \frac{\sqrt{2}}{\pi} V_{DC} \tag{2.40}$$

The load of the converter is composed of a single phase diode bridge and a battery pack, which can be modeled by a resistance (Figure 2.19). The output power can be expressed by:

$$P_{out} = V_{out} \cdot I_{out} \tag{2.41}$$

Using the FHA it is possible to write the voltage v_0 as a function of the amplitude of V_{out}:

$$v_0 = \frac{4}{\pi} V_{out} sin(2\pi f t - \phi) \tag{2.42}$$

where ϕ is the phase shift with respect to the input voltage. The rms value can be obtained by:

$$v_{0,rms} = \frac{2\sqrt{2}}{\pi} V_{out} \tag{2.43}$$

The value of the output current I_{out} corresponds to the mean value of the current rectified by the bridge rectifier:

$$I_{out} = \frac{2\sqrt{2}}{\pi} i_{0,rms} \tag{2.44}$$

at this stage the load will be modeled as a resistance, the output current is in phase with the output voltage so it is possible to calculate the equivalent resistance value at the bridge rectifier input:

$$R_{0,sec} = \frac{v_{0,rms}}{i_{0,rms}} = \frac{\frac{2\sqrt{2}}{\pi} V_{out}}{\frac{\pi}{2\sqrt{2}} I_{out}} = \frac{8}{\pi^2} R_{out} \tag{2.45}$$

To complete the model of the LLC converter, this analysis considers also the transformer ratio n to transport the value of the equivalent resistance to the primary side:

$$R_{0,eq} = n^2 \frac{8}{\pi^2} R_{out} \tag{2.46}$$

Based on (2.41), the equation 2.46 can be rewritten as:

$$R_{0,eq} = n^2 \frac{8}{\pi^2} \frac{V_{out}^2}{P_{out}} \tag{2.47}$$

Using the expression of the equivalent output resistance and the fundamental component of the input voltage it is finally possible to draw the equivalent circuit of the LLC converter (Figure 2.20).

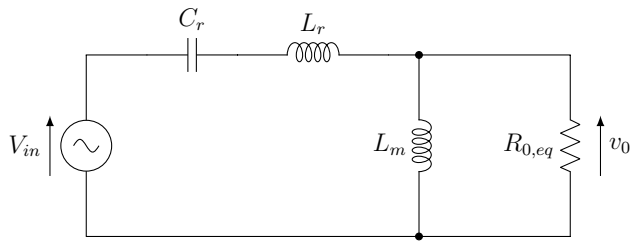

Figure 2.20: Equivalent circuit of the LLC converter using the FHA

2.2.2 Voltage transfer function of the LLC converter

Once the equivalent circuit of the LLC converter is retrived, the next step is to understand how the resonant tank affect the behavior of the transfer function between output voltage and input voltage.

The voltage gain $\bar{M}$ is given by the ratio of the output and input voltage, which are characterized by a magnitude and a phase. Consequently, also the voltage gain has its magnitude and phase and, as for the voltages, it can be represented by a complex number:

$$\bar{M} = n\frac{\bar{V}_0}{\bar{V}_{in}} \tag{2.48}$$

From now on, the analysis consider the a unitary turn ratio n. The results for different turn ratio value can be easily retrived accordingly. Considering the structure of the equivalent circuit, it is possible to write:

$$\bar{M} = \frac{1}{\frac{1}{s^2 C_r L_m} + \frac{1}{sC_r R_{0,eq}} + \frac{L_r}{L_m} + s\frac{L_r}{R_{0,eq}} + 1} \tag{2.49}$$

where s is the Laplace variable. The aim of the discussion is to find the Bode plot of $\bar{M}$, so s is replaced by$j\omega$:

$$\bar{M} = \frac{1}{-\frac{1}{\omega^2 C_r L_m} + \frac{1}{j\omega C_r R_{0,eq}} + \frac{L_r}{L_m} + j\omega\frac{L_r}{R_{0,eq}} + 1} \tag{2.50}$$

for better comprehension of the analysis, it is useful to define the following quantities:

- first resonance frequency:

$$f_{r,1} = \frac{1}{2\pi\sqrt{C_r L_r}} \tag{2.51}$$

- second resonance frequency:

$$f_{r,2} = \frac{1}{2\pi\sqrt{(L_r + L_m)C_r}} \tag{2.52}$$

- characteristic impedance:

$$Z_0 = \sqrt{\frac{L_r}{C_r}} = \frac{1}{2\pi f_{r,1} C_r} = 2\pi f_{r,1} L_r \tag{2.53}$$

- quality factor:

$$Q = \frac{Z_0}{R_0} = \frac{\pi^2}{8}\frac{I_{out}}{n^2 V_{out}} Z_0 = \frac{\pi^2}{8}\frac{P_{out}}{n^2 V_{out}^2} Z_0 \tag{2.54}$$

- inductance ratio:

$$\ell = \frac{L_r}{L_m} \tag{2.55}$$

- normalized frequency:

$$f_n = \frac{f}{f_{r,1}} \tag{2.56}$$

With these definitions, in is possible to write 2.50 in the following way:

$$\bar{M} = \frac{1}{\left(1 + \ell - \frac{\ell}{f_n^2}\right) + jQ\left(f_n - \frac{1}{f_n}\right)} \tag{2.57}$$

The voltage gain $\bar{M}$ is functions of three variables:

$$\bar{M} = f(f_n, Q, \ell) \tag{2.58}$$

As the amplitude of $\bar{M}$ represent the voltage gain, it is important to find its expression and to understand how the parameters of the LLC converter affect its characteristic. The amplitude of $\bar{M}$ can be computed from 2.57:

$$M = \frac{1}{\sqrt{\left(1 + \ell - \frac{\ell}{f_n^2}\right)^2 + Q^2\left(f_n - \frac{1}{f_n}\right)^2}} \tag{2.59}$$

the inductance ratio depends on the selected hardware and can be considered constant during operation. The voltage gain M depends on the switching frequency and on the quality factor Q (Figure 2.21). For small value of Q the peak of voltage gain, which occur at the second resonance frequency, is bigger while the amplitude at the first resonance frequency does not depend on the quality factor and it is always equal to 1. Moreover, when Q is small the characteristic is more sensitive to frequency variations for low f_n, but if the frequency is higher than the first resonance frequency the characteristic is flatter and it needs higher frequency values to reach a lower M value with respect to a characteristic with higher Q. In other words, if the value of Q is high the peak of voltage gain is smaller, but the characteristic does not require high frequency values to reach lower voltage gain.

For the sake of sizing the hardware components it is useful to plot the M characteristic for a fixed Q and different ℓ (Figure 2.22). For higher values of inductance ratio, higher voltage gains can be reached. However, high values of ℓ mean lower values of the magnetizing inductance L_m which causes an increase of the magnetizing current and higher power losses. So, the choice of ℓ value is a trade off between

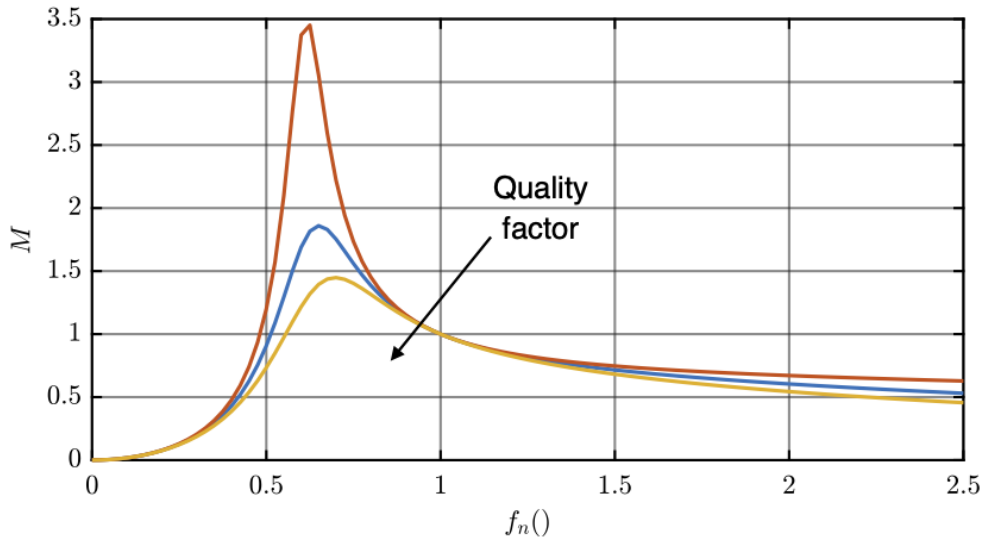

Figure 2.21: Different characteristics of voltage gain M depending on quality factor values

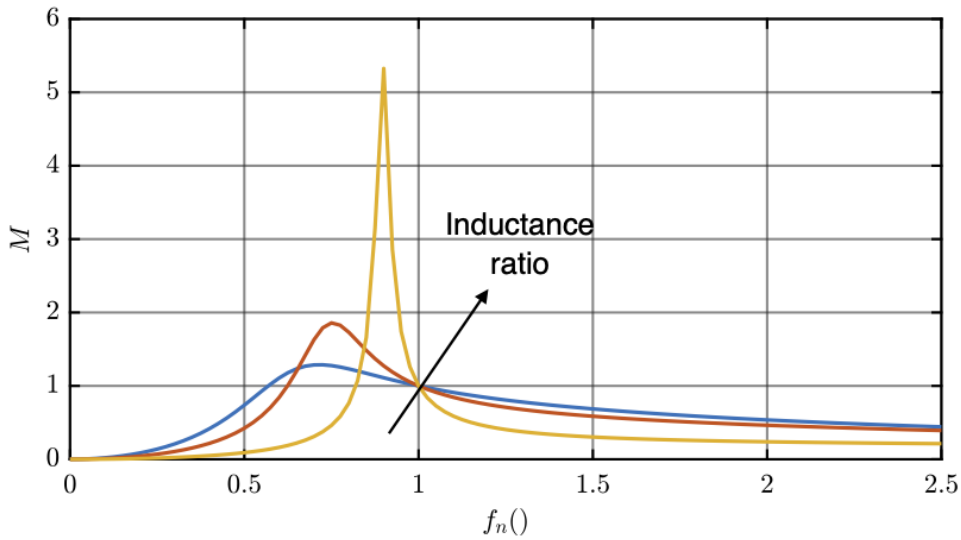

Figure 2.22: Different characteristics of voltage gain M depending on inductance ratio values

voltage range requirements and converter efficiency. Another aspect affected by the inductance ratio is the difference between the first and the second resonance frequency. With higher value of ℓ this difference is smaller and the characteristic is more sensitive to frequency variations.

Regardless the working point, which determine the value of Q, and the chosen value of ℓ it is possible to recognize two areas of the characteristic of the voltage gain, one for $M \geq 1$ and the other one for $M < 0$. This consideration means that the LLC converter can work both as step-up and step-down converter. It is worth at this point to notice that the previous voltage characteristic does take account of the voltage gain given by the transformer and its turns ratio can be designed to help the LLC converter to reach the required voltage gain.

2.2.3 Zero Voltage Switching

The LLC converter is used in applications requiring high efficiency. In fact, when the design of the LLC converter is well done the mosfets on the H-bridge converter are characterized by a Zero Voltage Switching, making the switching losses very small.

The ZVS operation [11] can be understood analyzing the waveform of current and voltage in the LLC converter during one switching period (Figure 2.23). The switching period can be divided into smaller time intervals:

- *Mode 1-2: Q_1,Q_4 ON and Q_2,Q_3 OFF.* The the input current flows through the resonant tank and becomes the primary side current of the transformer which is composed of the magnetizing current and the primary side load current. The current at the secondary side flows through D_5 and D_8 and the voltage applied to the output capacitor is applied also to the secondary side of the transformer, causing a voltage at the magnetizing inductance terminals equal to nV_{out}. As the output capacitance is assumed to be sufficiently high, the voltage applied to L_m result flat, causing a linear increasing of the magnetizing current. As the load current through the primary side is sinusoidal due to the resonant phenomena of the resonant tank, also the current through C_r and L_r has a form close to a sinusoidal wave. This mode finishes when the primary load current has reached the zero value.

- *Mode 2: Q_1,Q_4 ON and Q_2,Q_3 OFF.* The load current on the primary side has reached the zero value so only the magnetizing current is flowing through the circuit. It is important to note that for higher values of L_m, smaller values

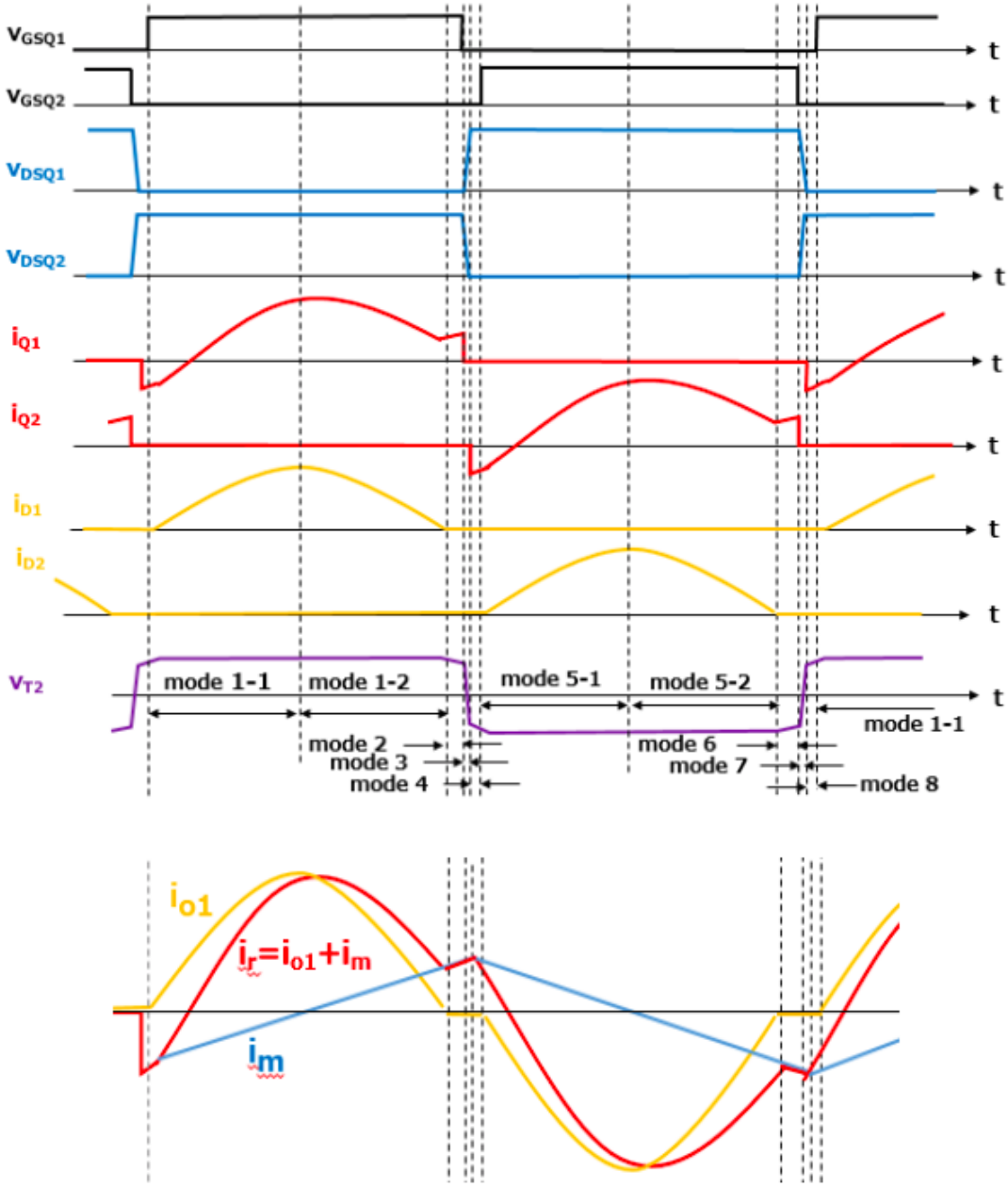

Figure 2.23: Waveforms of the electric quantities during a switching period in a LLC converter

of current flow through the circuit, improving the converter efficiency. Then, Q_1 and Q_4 turn OFF and the mode finishes when the current through them

reach the zero value

- *Mode 3: Q_1,Q_2,Q_3,Q_4 OFF.* In this interval of time the parasitic capacitance of the power switches play a key role. In fact, as Q_1 and Q_4 turn OFF the magnetizing current keep flowing through the transformer via the parasitic capacitance of the power switching, causing the voltages Q_1 and Q_4 to increase and Q_2 and Q_3 to decrease. This mode finishes when the charging and discharging of the capacitances is complete.

- *Mode 4: Q_1,Q_2,Q_3,Q_4 OFF.* When the charging operation of capacitance C_2 and C_3 is complete the diodes D_3 and D_4 result forward biased and they begin to conduct. This mode finishes when Q_2 and Q_3 turn ON.

- *Mode 5-1: Q_1,Q_4 OFF and Q_2,Q_3 ON.* At the beginning of this time interval diodes D_2 and D_3 are in a conductive state, so mosfet Q_2 and Q_3 are turned ON under ZVS condition. As Q_2 and Q_3 turn ON, C_r act as a voltage source due to the stored energy and it causes a current to flow in the opposite direction. In this way, the load current on the primary side of the transformer assume negative values causing D_6 and D_7 to conduct. As a consequence, a negative voltage is applied to L_m that decrease the value of the magnetizing current. This mode finish when the magnetizing current reach zero and revers its polarity.

- *Mode 5-2: Q_1,Q_4 OFF and Q_2,Q_3 ON.* The magnetizing current continues to increase in negative direction. This mode is the same as Mode 1-2, but with reversed polarity of the electric quantities.

After Mode 5-2, the trend of currents and voltages is the same as described in the previous Modes, the only difference is the polarity of their values. Also the behavior of the power switch is the same.

The ZVS can be identified in Mode 3 and in Mode 5-1. At the beginning of Mode 3 switches Q_1 and Q_4 turn OFF and this transition happen in a ZVS condition. In fact, before the turn OFF the voltage applied to the switch is very small and equal to the voltage drop of the conducting state. When the switches turn OFF, the value of the voltage is kept almost constant due to the parasitic capacitance. So,

if the value of parasitic capacitance is high enough, the current through the switch can reach zero while the voltage is still close to zero. When the current through the switch reach zero, the current of the resonant tank start to flow through the parasitic capacitance increasing the voltage at the terminals of the power switch. In this way, during the switching time interval, there are not contemporary values of current and voltage thus ensuring a very low switching loss.

Considering Mode 5-1 it is possible to note that when Q_2 and Q_3 turn ON, their body diodes D_2 and D_3 are already in a conducting condition so the voltage applied to their terminal was close to zero. Consequently, the current through the power switch can increase while the voltage at its terminals is close to zero.

It is important to note that the current of the resonant tank lags the voltage given by the bridge inverter. This is an essential requirement to make the ZVS happen.

2.2.4 The equivalent input impedance

As the ZVS require an inductive behavior, the next step is to analyze the equivalent input impedance and defining the border line between the capacitive and inductive behavior.

Considering the equivalent circuit of the LLC converter (Figure 2.20), the input impedance can be calculated using:

$$\bar{Z}_{in} = \frac{1}{sC_r} + sL_r + \frac{sR_{0,eq}L_m}{R_{0,eq} + L_m} \tag{2.60}$$

2.60 can be normalized with respect to the characteristic impedance Z_0:

$$\bar{Z}_n = \frac{\bar{Z}_{in}}{Z_0} \tag{2.61}$$

Using 2.51, 2.53, 2.54, 2.55 and 2.56, 2.61 can be written as follow:

$$\bar{Z}_n(f_n, Q, \ell) = \frac{Qf_n^2}{\ell^2 + Q^2 f_n^2} + j\left(\frac{f_n \ell}{\ell^2 + Q^2 f_n^2} - \frac{1 - f_n^2}{f_n}\right) \tag{2.62}$$

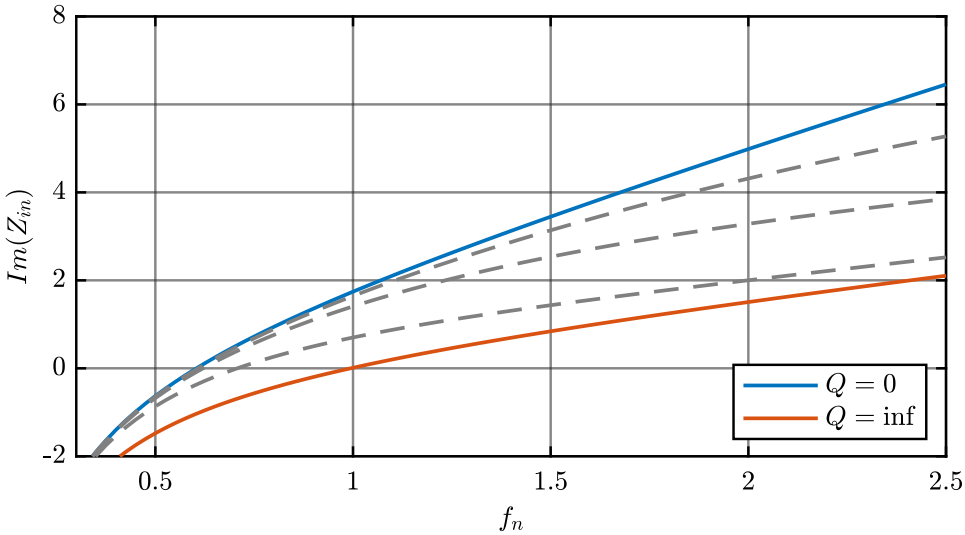

Figure 2.24: Trend lines of the imaginary part of the input impedance as function of the switching frequency

Equation 2.62 is very important because it shows the real and imaginary parts of the input impedance, which determines the behavior of the LLC converter.

If the components of the resonant tank are know, the imaginary part of 2.62 depends on Q and f_n (Figure 2.24). There are two border lines: one referred to the short circuit condition and the other one referred to the open circuit condition. Between these border lines there are all the possible values of the imaginary part of the input impedance. It is possible to see that the inductive behavior is always ensured when the switching frequency is higher than the first resonance frequency. Likewise, the LLC converter always assumes a capacitive behavior when the switching frequency is lower than the second resonance frequency.

The limit condition in which the ZVS is still ensured occurs when the imaginary part of 2.62 is equal to zero:

$$\frac{f_n \ell}{\ell^2 + Q^2 f_n^2} - \frac{1 - f_n^2}{f_n} = 0 \tag{2.63}$$

Assuming that the working point and the parameters of the LLC converter are

know, the only unknown variable in 2.63 is f_n, which can be evaluated using:

$$f_{n,lim} = \sqrt{\frac{Q^2 - \ell(1+\ell) + sqrt[\ell(\ell+1) - Q^2]^2 + 4Q^2\ell^2)]}{2Q^2}} \tag{2.64}$$

Likewise, if in 2.63 the frequency and the inductance ratio are know, it is possible to retrive the limit value of the quality factor:

$$Q_{lim} = \sqrt{\frac{\ell}{1-f_n^2} - \left(\frac{\ell}{f_n}\right)^2} \tag{2.65}$$

which is valid for:

$$\sqrt{\frac{\ell}{\ell+1}} < f_n < 1 \tag{2.66}$$

The limit of the voltage gain is retrived by using (2.65) in (2.59):

$$M_{lim} = \frac{f_n}{\sqrt{f_n^2(1+\ell) - \ell}} \tag{2.67}$$

It should be remarked that expression (2.67) is valid for values of switching frequency between the first and the second resonance frequency. In fact, as mentioned before, for values of frequency higher than the first resonance frequency the behavior of the LLC converter is always inductive, so the ZVS is always possible.

2.2.5 Step-up and Step-down functioning

In previous subsections the voltage gain has been analyzed and it is possible to see that its trend line assumes values below and above the unitary value depending on the switching frequency. So it is interesting to understand how the LLC converter works for values of the switching frequency above, below and equal to the first resonance frequency.

For values below the resonance frequency the LLC converter works as a step-up (boost) converter (Figure 2.26). In this condition there are two freewheeling

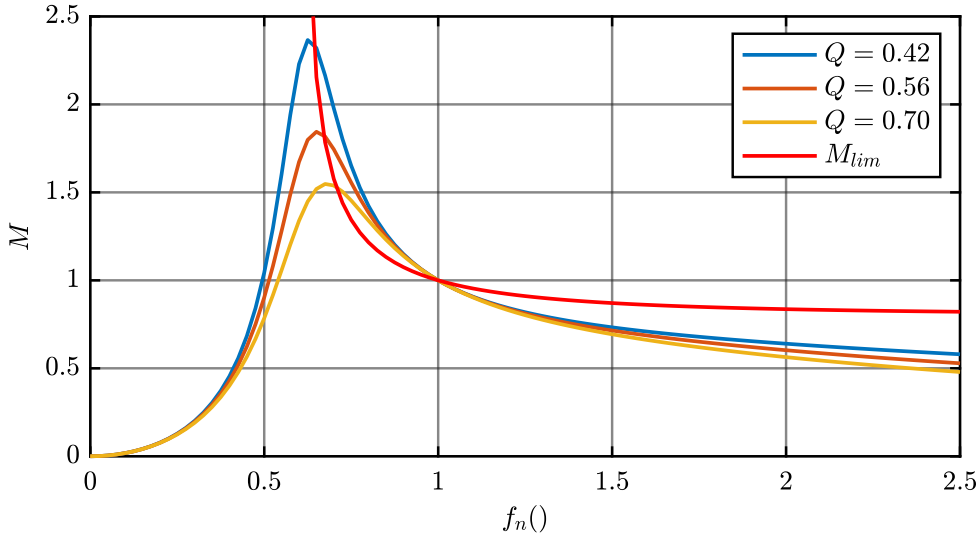

Figure 2.25: Representation of the limit value of the voltage gain

operations every switching period. In fact, as the resonance frequency is higher than the switching frequency, the current flowing through the L_r reaches the same value of the magnetizing current before that the half switching period ends. This leads to a zero current on the secondary side of the transformer and L_m starts to resonate with the other capacitor. As the second resonance frequency is lower than the first one, the current through the inductors remains almost constant. In boost condition, the diodes of the bridge rectifier works with Zero Current Switching (ZCS) as their current reaches zero before the next half switching period.

When the switching frequency is equal to the first resonance frequency the LLC converter works in the best condition (Figure 2.27). The current flowing through L_r reaches the same value of the magnetizing current exactly at the end of the half switching period and it has a perfect sinusoidal form. In this case there are no freewheeling operations, but still the diodes of the bridge rectifier work in a ZCS condition.

For values of switching frequency above the first renonant frequency the LLC converter works as a step-down (buck) converter (Figure 2.28). As the switching frequency is higher than the first resonance frequency, the current through the inductor L_r can not reach the same value of the magnetizing current before the end of the half switching period. When the polarity of the input voltage is reversed,

the current through L_r rapidly decrease to reach the magnetizing current. In this condition the diodes of the bridge rectifier are hard switched as the current does not reach zero before the end of the half switching period.

2.2.6 Control strategy for the LLC converter

Once the transfer function of the voltage gain M is understood it is possible to implement a control scheme in order to properly manage the battery charging. From the specifications of the project, the following characteristics of the battery pack are identified:

- $V_{batt,n}$: nominal battery voltage
- $V_{batt,f}$: voltage of at the battery terminals when fully recharged
- $I_{batt,n}$: nominal recharging current
- $P_{r,max}$: maximum recharging power

The maximum power is reached when current and voltage assume their maximum values at the same time, which occur on the transition between the constant current interval and the constant voltage interval:

$$P_{r,max} = V_{batt,f} \cdot I_{batt,n} \tag{2.68}$$

As the converter is designed for a specific range of power and the battery voltage is given by its datasheet, it is possible to retrive the nominal current of the battery recharge:

$$I_{batt,n} = \frac{P_{r,max}}{V_{batt,f}} \tag{2.69}$$

A cascaded control is used to realize the required charging profile. An inner current loop is used to control the battery current while an outer voltage loop is dedicated to control the battery voltage and to determine the current reference value of the current loop (Figure 2.29).

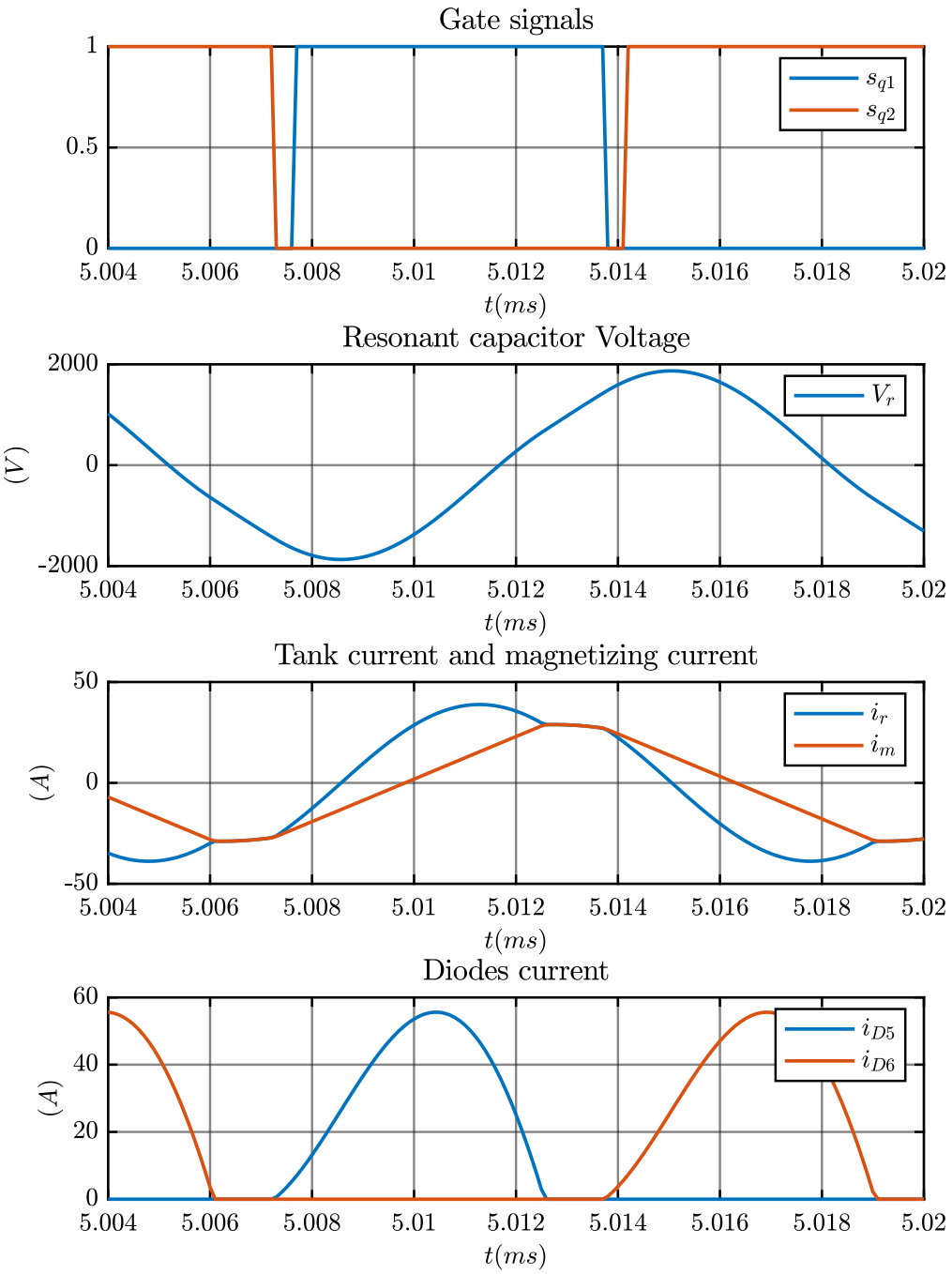

Figure 2.26: LLC waveforms in boost mode

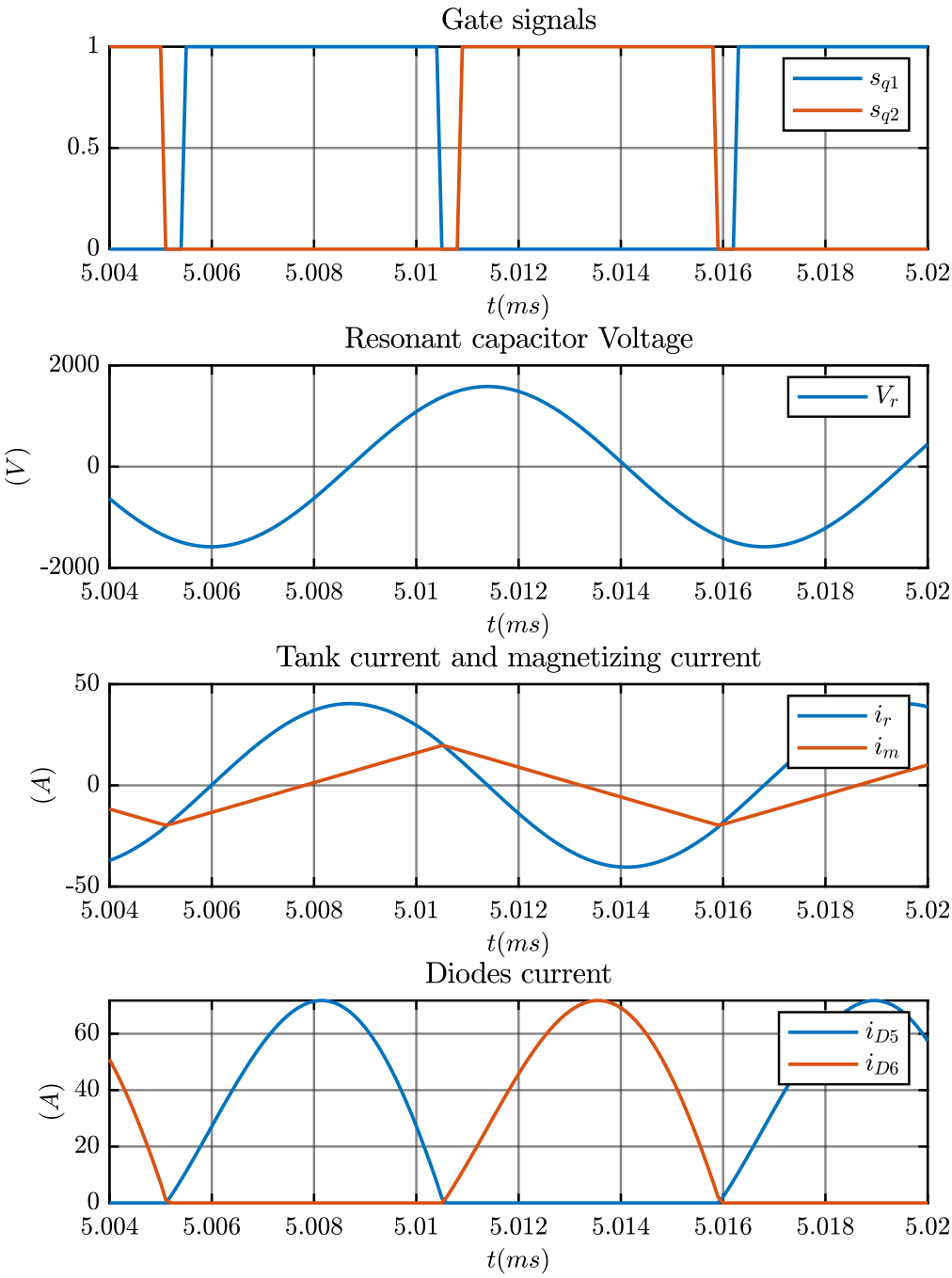

Figure 2.27: LLC waveforms in first resonant mode

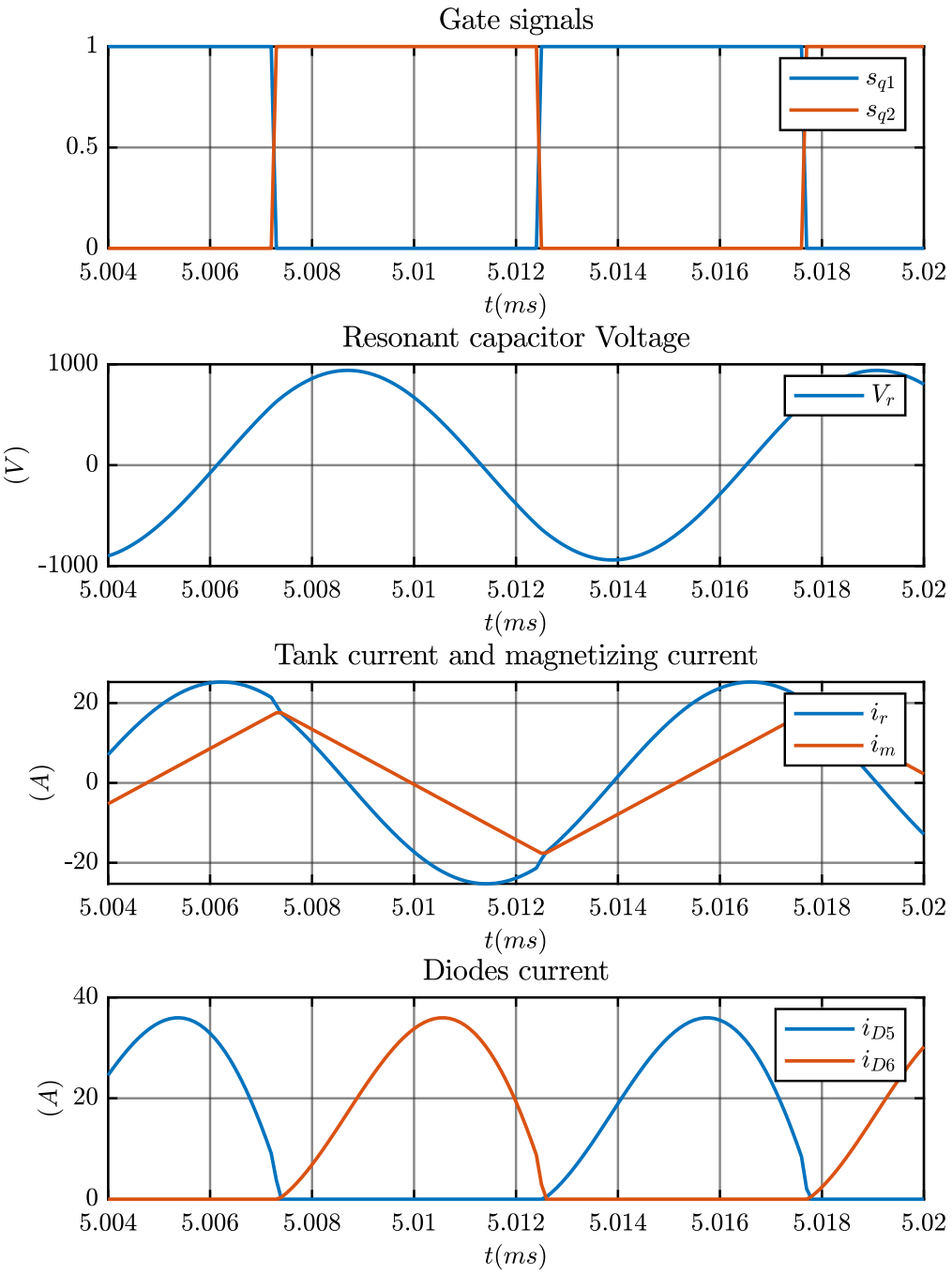

Figure 2.28: LLC waveforms in buck mode

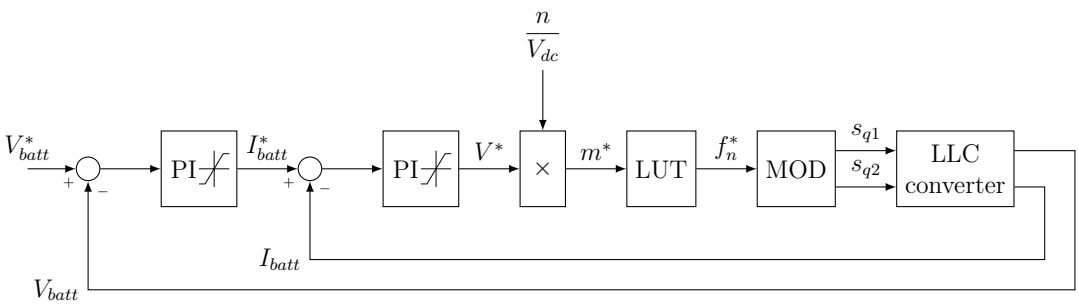

Figure 2.29: Control scheme of the LLC converter

The input of the control scheme is the desired battery voltage V^*_{batt} that is equal to the value of the battery voltage when it is fully charged. This value is compared with the actual value V_{batt} at the battery terminals and the difference is sent to the PI regulator. The output of the PI is saturated to the nominal current value $I_{batt,n}$ and it represent the desired current I^*_{batt} through the battery. The difference between I^*_{batt} and the actual value I_{batt} is sent to another PI and its output represent the required voltage V^* at the LLC output terminals. This value is then multiplied for the turns ratio n of the transformer and divided by the measured nominal input voltage V_{dc}, which is the voltage on the DC link. At this point the required voltage gain m^* is found and it is sent to a Look-Up Table (LUT) giving at its output the required normalized switching frequency f^*_n. The last control block is the modulation block (MOD) which determines the gate signal of the bridge inverter depending on the value of f^*_n. Finally, the measured values of current I_{batt} and voltage V_{batt} are retrived from the output of the LLC converter, which is connected to the battery pack.

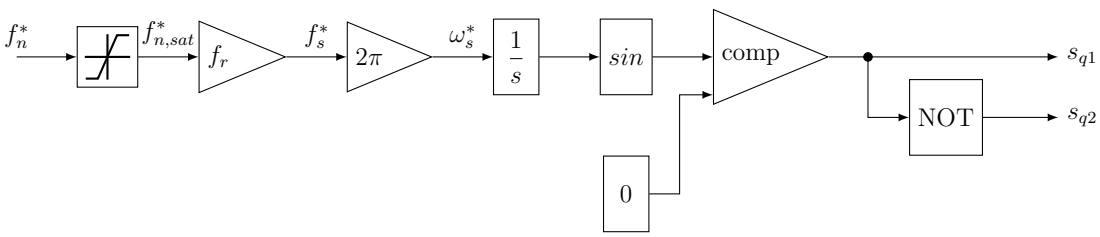

Figure 2.30: Modulation block of the LLC control scheme

The modulation block (Figure 2.30) takes as input the required switching frequency f_n^* and the first thing it does is to saturate this value between the maximum and the minimum normalized switching frequency in which the LLC converter works. The saturated switching frequency is then multiplied for $2\pi f_{r,1}$ to give the real value ω^* of the desired switching frequency. The reference frequency is integrated to obtain a fictitious position signal. The square wave gate signals s_{q1} and s_{q2} are obtained by comparing the sine of this fictitious angle with zero. As the duty cycle of the bridge inverter is always equal to 0.5, s_{q1} is ON during the first half period of the sinusoidal signal and s_{q2} is ON during the second half period. To complete the modulation block, the dead time are introduced for the turn ON of the gate signals.

As the output filter introduces an inductor in series with the battery pack, the parameter of the current PI can be easily tuned as follow:

$$k_{p,i} = \omega_{b,i} \cdot L_{out} \tag{2.70}$$

$$k_{i,i} = \omega_{b,i} \cdot k_{p,i} \tag{2.71}$$

where:

- $\omega_{b,i}[rad/s]$ is the bandwidth of the current loop
- $L_{out}[H]$ is the output inductance given by the filter

In order to determine the parameters of the voltage PI two assumption are considered:

1. the output current ripple is very small
2. the battery is considered as a capacitor with a very high capacitance value

With this assumption it is possible to consider the transfer function between output current and output voltage as follow:

$$\frac{I_{batt}(s)}{V_{batt}(s)} = sL_{out} + \frac{K}{sC_{batt}} + R_b \approx R_b \tag{2.72}$$

where:

- $R_b[\Omega]$ is the equivalent series resistance of the battery pack
- K is a coefficient that depends on the battery characteristics
- $C_{tot}[F]$ is the equivalent capacitance of the battery pack

2.72 is justified by the fact that the ripple current is very small so the voltage drop due to L_{out} is very small and the equivalent battery capacitance C_{tot} is very high. Consequently, both of the voltage terms due to these parameters can be neglected. The parameters of the voltage PI are then tuned as follow:

$$\omega_{b,v} = 0.1 \cdot \omega_{b_i} \tag{2.73}$$

$$k_{p,v} = 0 \tag{2.74}$$

$$k_{i,v} = \frac{\omega_{b,v}}{R_b} \tag{2.75}$$

All the control bandwith of the converters control are summarized in Table 2.1.

		T-type	LLC
Sampling frequency	f_s	20kHz	20kHz
Current control bandwidth	f_i	1kHz	1kHz
Voltage control bandwidth	f_v	5Hz	10Hz

Table 2.1: Bandwidths of the control loops

Chapter 3

Preliminary design of the battery charger

At this point the working principles of the T-type and of the LLC converter are known so it is possible to design the battery charger in order to satisfy the specifications of the project. The first step is to design the components of the T-type converter because it establishes the grid connection and the voltage value on the DC-link. After the design of the T-type converter it is possible to design the components of the LLC converter.

The design made in this chapter is just preliminary and the results will be used for the first simulations via software. The simulations will successively help to find the final components of the two converters.

3.1 Design of the T-type converter

The first thing to do is to decide the DC-link voltage value and then it is possible to design all the T-type converter components:

- input inductors
- output capacitors
- power mosfets

- power diodes

As said in the previous chapter, the functioning of the T-type converter is similar to a boost converter so half of the DC-link voltage value V_{dc}must be higher than the peak of the input voltage V_{in}:

$$\frac{V_{dc}}{2} \geq \sqrt{2}V_{in,rms} = \sqrt{2} \cdot 220 = 311V \tag{3.1}$$

The chosen value of the DC-link voltage is $800V$.

3.1.1 Design of the output capacitors

Once the DC-link voltage value is established, it is easy to determine the nominal voltage $V_{c,n}$ of the output capacitors:

$$V_{c,n} \geq \frac{V_{dc}}{2} = 400V \tag{3.2}$$

The capacitance values are chosen with the aim to reduce the voltage ripple on the DC-link. Considering the boost functioning:

$$\frac{v_c}{v_{in}} = \frac{1}{1 - d(t)} \tag{3.3}$$

$$\frac{i_{dc}}{i_{in}} = 1 - d(t) \tag{3.4}$$

where the input voltage is given by:

$$v_{in} = \hat{V}_{in} sin(\omega t) \tag{3.5}$$

Recombining these equations it is possible to write:

$$i_{dc}(t) = \frac{\hat{V}_{in}}{V_c}\hat{I}_{in}(sin\omega t)^2 = \frac{1}{2}\frac{\hat{V}_{in}}{V_c}\hat{I}_{in}\frac{1}{2}\frac{\hat{V}_{in}}{V_c}\hat{I}_{in}cos(2\omega t) \tag{3.6}$$

3.6 shows that the current on the DC-link is composed of one mean term and one sinusoidal term which is characterized by the double of the input frequency. The sinusoidal term will introduce a voltage ripple on the output capacitor at the same frequency. Its peak value is given by:

$$\hat{V}_{dc,2nd} = \frac{1}{2\omega C_{out}} \hat{I}_{dc,2nd} = \frac{\hat{I}_{in}}{4\omega C_{out}} \frac{\hat{V}_{in}}{V_c} \tag{3.7}$$

Consequently, the capacitance value of each output capacitor can be calculated by assuming a maximum value of the voltage ripple:

$$C_{out} = \frac{\hat{I}_{in}}{4\omega \hat{V}_{dc,2nd}} \frac{\hat{V}_{in}}{V_c} \tag{3.8}$$

As a matter of fact, the LLC converter is very sensitive to voltage variations at its input terminals, so the ripple voltage at the DC-link should be very small. The chosen value of $V_{dc,2nd}$ is the equal to $8V$ which correspond to 1% of the nominal DC-link voltage. The other required values are equal to:

- $\hat{I}_{in} = \frac{P_{n,1ph}}{V_{in}} \sqrt{2} = \frac{6000}{220} \sqrt{2} = 38.7A$
- $V_c = 400V$
- $\hat{V}_{in} = \sqrt{2} \cdot 220 = 311.12V$
- $\omega = 2\pi f = 2\pi \cdot 50 = 314.16 rad/s$

Substituting these values in 3.8, it is possible to find the output capacitance value:

$$C_{out} = \frac{38.7 \cdot 311.12}{4 \cdot 314.16 \cdot 8 \cdot 400} = 3mF \tag{3.9}$$

3.1.2 Design of the input inductors

The standard requirements splits into two different approaches depending on the value of the input current: in the first case the input current is higher than $16Arms$ and the limit value of THD can not be exceed, in the second case the input current is lower than $16Arms$ and the peak of harmonics components can not exceed specific

limits. The most difficult part in satisfying the requirements is to have a THD not higher than the standard limit when its value is exactly $16Arms$.

The current THD is defined as:

$$THD = \frac{\sqrt{\sum_{n=2}^{\infty} I_{n,rms}^2}}{I_{fund,rms}} \tag{3.10}$$

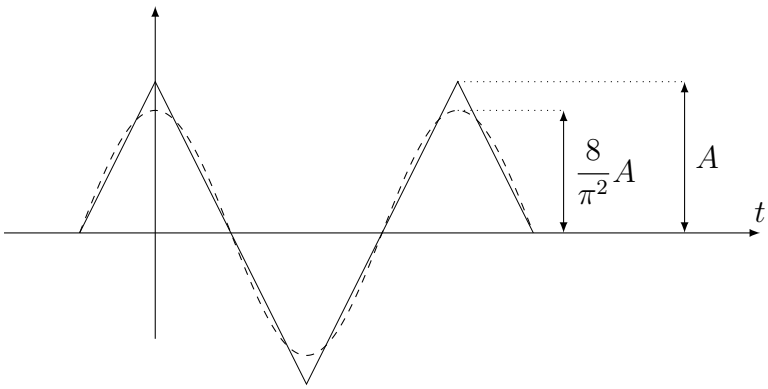

Figure 3.1: Triangular wave and its first harmonic component

A first try value for the input inductor is calculated considering the input current as a sine wave with a triangular ripple due to the switching process. The fourier series of a triangular wave is given by:

$$tr(t) = \sum_{n=1}^{\infty} a_n cos(n\omega_0 t) \tag{3.11}$$

where:

$$a_n = \begin{cases} 4A\dfrac{1-(-1)^n}{\pi^2 n^2}, & \text{n odd} \\ 0, & \text{n even} \end{cases} \tag{3.12}$$

The coefficient A is the magnitude of the triangular wave (Figure 3.1). The current

ripple assume a symmetric shape when the duty cycle is equal to 0.5 and the peak-to-peak value reach its maximum value which can be calculated using [10]:

$$\Delta_{i,pp} = \frac{V_{out}}{4 f_{sw} L_{in,eq}} \tag{3.13}$$

where:

- $L_{in,eq}[H]$ is the equivalent input inductance
- $f_{sw}[Hz]$ is the switching frequency
- $V_{out}[V]$ is the output voltage of the single converter structure and in this application corresponds to $\frac{V_{dc}}{2}$

As A is equal to half of the peak-to-peak value of the ripple current, it is possible to write:

$$A = \frac{\Delta_{i,pp}}{2} = \frac{V_{out}}{8 f_{sw} L_{in}} \tag{3.14}$$

Considering just the first harmonic component of the triangular wave it is possible to substitute 3.12 into 3.10:

$$THD = \frac{8A}{\sqrt{2}\pi^2 I_{fund,rms}} \tag{3.15}$$

Finally, substituting 3.14 into 3.15 it is possible to retrive the first try value of $L_{in,eq}$:

$$L_{in} = \frac{V_{out}}{\sqrt{2}\pi^2 I_{fund,rms} f_{sw} THD} \tag{3.16}$$

Considering the following values:

- $V_{out} = 400V$
- $I_{fund,rms} = 16Arms$

- $f_{sw} = 20kHz$
- $THD = 0.23$

3.16 will give:

$$L_{in,eq} = 390\mu H \tag{3.17}$$

The single-phase configuration of the T-type converter works with the three phases connected in parallel, so the inductance for each phase must be equal to:

$$L_{in} = 1.17mH \tag{3.18}$$

Obviously, this is a precautionary value as the interleaved control has not been taken into account to reach this result and the expectations is to reduce this value for the final design. This is just a starting point value and the simulations via software will help to improve the design.

Regarding the choice of the nominal current, it is possible to verify that in the three phase configuration the current that flow through the input inductors is higher than in the single-phase configuration:

$$I_{L,3ph} = \frac{P_{n,3ph}}{3V_{in}} = \frac{11000}{3 \cdot 220} = 16.7A \tag{3.19}$$

$$I_{L,1ph} = \frac{I_{in}}{3} = \frac{P_{n,1ph}}{3V_{in}} = 9.1A \tag{3.20}$$

So the nominal current of the inductors must be higher than $16.7A$.

3.1.3 Choice of the semiconductor devices

The last step of the preliminary design of the T-type converter is to choose the semiconductor devices. As mentioned before, the three-phase configuration is the one with higher current on each phase so it determines the reference value for the nominal current of diodes and mosfets. The diodes must withstand a reverse voltage equal to the entire DC-link voltage value. Conversely, the mosfet on the middle

legs must withstand just half of the DC-link voltage because they are connected in series. These considerations permit the choice of the diodes and mosfets.

	Diodes	Mosfet
$I_n[A]$	≥ 16.7	≥ 16.7
$V_r[V]$	≥ 800	≥ 400

Table 3.1: Values of nominal current and reverse voltage for the choice of diodes and mosfet in the T-type converter

3.2 Design of the LLC converter

The most important part of the LLC converter design is to determine parameters of the resonant tank and of the transformer, because they affect the voltage gain between input and output. Once they are determined it is possible to continue with the design of the resonant inductor and of the transformer. Finally, some considerations are made about the output filter.

3.2.1 Design of the resonant tank

The design of the resonant tank has been already treated in previous works ([12]) and can be divided into the following steps:

1. Define all the specifications of the LLC conveter:

Minimum battery voltage	$V_{batt,min}$	350	$[V]$
Maximum battery voltage	$V_{batt,max}$	420	$[V]$
Minimum DC-link voltage	$V_{dc,min}$	792	$[V]$
Maximum DC-link voltage	$V_{dc,max}$	808	$[V]$
Maximum recharging power	P_{max}	$11 \cdot 10^3$	$[W]$
First resonant freqeuncy	$f_{r,1}$	$100 \cdot 10^3$	$[Hz]$
Maximum switching frequency	f_{max}	$130 \cdot 10^3$	$[Hz]$
Maximum dead time	$t_{d,max}$	$50 \cdot 10^{-9}$	$[s]$
Output mosfet capacitance	C_{oss}	$56 \cdot 10^{-12}$	$[F]$
Efficiency	η	0.95	[]

Table 3.2: Specifications for the resonant tank design

2. Find the transformer turn ratio:

$$n = \frac{V_{dc,min}}{V_{batt,min}} \tag{3.21}$$

Using 3.21, the minimum voltage gain is required when the input voltage is at its maximum value and the desired battery voltage is at its minimum, while the maximum voltage gain is required when the battery voltage is at its maximum and the input voltage is at its minimum.

3. Define the maximum and the minimum voltage gains:

$$M_{max} = \frac{nV_{batt,max}}{V_{dc,min}} \tag{3.22}$$

$$M_{min} = \frac{nV_{batt,min}}{V_{dc,max}} \tag{3.23}$$

4. Define the inductance ratio ℓ:

$$\ell = \left(\frac{1}{M_{min}} - 1\right)\frac{8f_{max}^2}{8f_{max}^2 - \pi^2} \tag{3.24}$$

In order to be able to control the current down to zero it is necessary to verify:

$$M(1+\ell) \geq 1 \tag{3.25}$$

5. Determine the limit conditions for the ZVS in boost mode:

$$M_{crit} = \sqrt{1 + \sqrt{\frac{\ell}{\ell+1}}} \tag{3.26}$$

$$Z_{0,crit} = \frac{8V_{dc,min}^2}{\pi^2 P_{out,max}}\left(\sqrt{\ell(1+\ell)} + \ell\right) \tag{3.27}$$

The LLC converter works in the limit condition for the ZVS when the characteristic impedance is equal to $Z_{0,crit}$ and the battery voltage determine a voltage gain equal to M_{crit}. In this conditions the input and output currents are equal to:

$$I_{batt,crit} = \frac{nP_{out,max}}{M_{crit}V_{dc,min}} \tag{3.28}$$

$$I_{dc,crit} = \frac{P_{out,max}}{\eta V_{dc,min}} \tag{3.29}$$

6. The expressions in the previous step are related to the inductance ratio so it is possible to determine the magnetizing inductance:

$$L_m = \frac{n^2}{f_{r,1}}\frac{M_{crit}\frac{V_{dc,min}}{n}}{4nI_{dc,crit} + (\pi^2\ell M_{crit} - 4)I_{batt,crit}} \tag{3.30}$$

7. Verify if the value of the magnetizing inductance is not too high:

$$L_m \leq \frac{t_{d,max}}{8\pi f_{r,1} C_{oss}} \sqrt{\left(1 + \frac{1}{\ell}\right) M_{min}^2 - dfrac1\ell(1+\ell)} \tag{3.31}$$

This check is done considering the maximum switching frequency and power equal to zero delivered to the battery. In this condition the current that flow through the resonant tank is equal to the smallest possible value. If L_m is too high, the current is not high enough to charge and discharge the parasitic capacitance of the mosfets, so the ZVS is not ensured.

8. Once the inductance ratio and the magnetizing inductance are determined, it is possible to retrive the other parameters of the resonant tank:

$$L_r = \ell L_m \tag{3.32}$$

$$C_r = \frac{1}{4\pi^2 f_r^2 L_r} \tag{3.33}$$

$$f_{r,2} = \frac{1}{2\pi\sqrt{(L_m + L_r)C_r}} \tag{3.34}$$

$$Z_0 = \frac{L_r}{C_r} \tag{3.35}$$

The value of the characteristic impedance Z_0 must not exceed its critical value $Z_{0,crit}$:

$$Z_0 \leq Z_{0,crit} \tag{3.36}$$

9. The minimum switching frequency is the lower value in which the ZVS must be ensured. Once the maximum value of voltage gain is determined, it is possible to substitute it into 2.67 and to retrive the value of minimum switching

frequency:

$$f_{n,min} = \frac{1}{\sqrt{1 + \frac{1}{\ell}\left(1 - \frac{1}{M_{max}^2}\right)}} \tag{3.37}$$

10. Finally, it is necessary to check if the maximum value that the quality factor can assume during the converter functioning does not exceed the limit value for the ZVS Q_{lim}:

$$Q_{max} \leq Q_{lim} \tag{3.38}$$

The limit value can be retrived by substituting 3.37 into 2.65:

$$Q_{lim} = \frac{\ell}{M_{max}\sqrt{\frac{1}{\ell} + \frac{M_{max}^2}{M_{max}^2 - 1}}} \tag{3.39}$$

The maximum value that the quality factor can assume during the converter functioning is given by:

$$Q_{max} = \frac{\pi^2 n^2}{8} \frac{I_{batt,max}}{V_{in,min}} Z_0 \tag{3.40}$$

If the conditions given in steps 4, 7, 8, and 10 are not satisfied it is necessary to modify the value of the inductance ratio ℓ.

The results of this procedure havee been calculated by using a MATLAB Script and they are reported in Table 3.3.

3.2.2 Design of the resonant inductor

The procedure followed for the design of the resonant inductor is described in [13].

The selected shape of the core is the PQ shape as this topology is designed specially for switching mode power supply and they optimize the ratio of core

turns ratio	n	2	[ ]
maximum voltage gain	M_{max}	1.0606	[ ]
minimum voltage gain	M_{min}	0.8663	[ ]
inductance ratio	ℓ	0.5714	[ ]
magnetizing inductance	L_m	108	$[\mu H]$
resonant inductance	L_r	62	$[\mu H]$
resonant capacitance	C_r	41	[nF]
characteristic impedance	Z_0	38.74	$[\Omega]$
minimum switchin frequency	f_{min}	95.346	$[kHz]$

Table 3.3: Results of the LLC converter design

volume to winding and surface area. The material of the core is Ferrite T, which is suited for Automotive applications.

The design procedure is divided into the following steps:

1. Compute the LI^2 product:

$$LI^2 = L\left(\frac{1.5 \cdot P_{max}}{V_{dc}}\right)^2 = 62 \cdot 10^{-6}\left(\frac{1.5 \cdot 11000}{800}\right)^2 = 20mJ \tag{3.41}$$

   Note that a precautionary margin for the value of current has been taken into account.

2. Select the core model using the Ferrite Core Selector chart (Figure 3.2) and read the nominal inductance A_L. The core model chosen for the resonant inductor is *PQ44040* ([14], Figure 3.3) and its nominal inductance is equal to $A_L = 150mH/1000turns$

3. Calculate the number of turns:

$$N = 10^3\sqrt{\frac{L}{A_L}} = 10^3\sqrt{\frac{62 \cdot 10^{-6}}{150 \cdot 10^{-3}}} = 20 \tag{3.42}$$

Once the core model is selected it is possible to design the winding of the inductor. Litz wire is used for this purpose because their are designed for high frequency

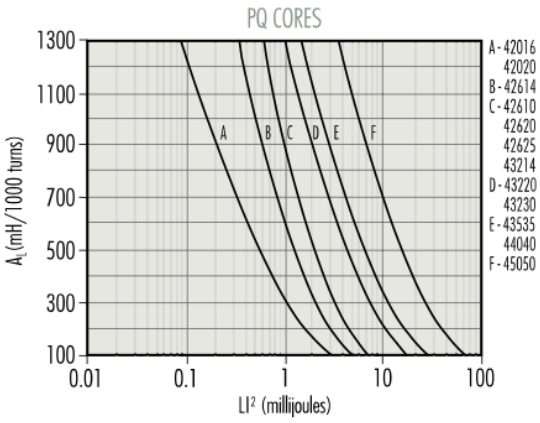

Figure 3.2: MAGNETICS Ferrite Core Selector chart for PQ shape

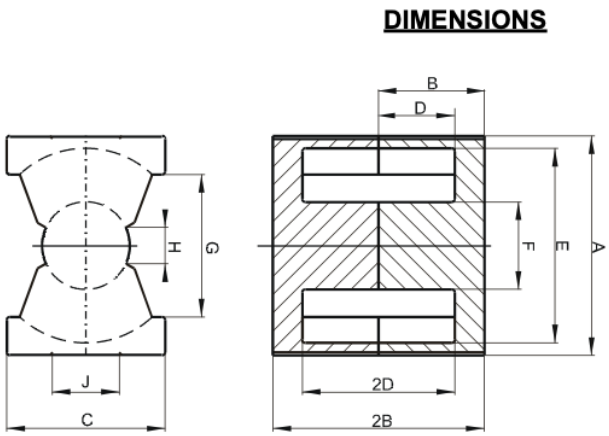

(mm)	Nominal:	Tol. min.:	Tol. max.:
A	41.5	-0.9	+ 0.9
B	19.9	-0.15	+ 0.15
2B	39.8	-0.30	+ 0.30
C	28.0	-0.6	+ 0.6
D	14.75	-0.20	+ 0.20
2D	29.5	-0.4	+ 0.4
E	37.0	-0.6	+ 0.6
F	14.9	-0.30	+ 0.30
G	28.0 Min.		
H	6.05 Min.		
J	15.0 Min.		
Eff. Parameters			
Ae mm ²	Amin mm ²	le mm	Ve mm ³
201	175	102	20500

Figure 3.3: MAGNETICS Core PQ44040

applications and they are able to minimize the skin effect.

Assuming a fill factor f_{Cu} equal to 0.4 it is possible to calculate the copper section of the inductor winding:

$$A_{Cu} = (E - F) \cdot 2D \cdot f_{Cu} = (37 - 14.9) \cdot 29.5 \cdot 0.4 = 260mm^2 \tag{3.43}$$

The section of the single wire is retrived dividing the last expression by the number

of turns:

$$S_{Cu} = \frac{A_{Cu}}{N} = 13mm^2 \tag{3.44}$$

The chosen value of the wire section is $10mm^2$ that is a bit smaller than the value in 3.44. This solution is better in term of weight and it permits to have a good value of current density anyway.

It is useful to calculate the winding resistance of the resonant inductor at the rated temperature, which is assumed to be $120^{\circ}C$. This value will be used to calculate the power losses of the converter. The winding resistance can be calculated by using:

$$R_{Lr} = \rho_{120}\frac{N\ell}{S_{Cu}} \tag{3.45}$$

where:

- $\rho_{120} = 0.0244[\Omega mm^2/m]$ is the copper resistivity at $120^{\circ}C$
- $N = 20$ is the number of turns of the winding
- $\ell = 116mm$ is the mean length of the winding turns
- $S_{Cu} = 10mm^2$ is the section of the winding wires

Substituting in (3.45) it is possible to obtain:

$$R_{Lr} = 4m\omega \tag{3.46}$$

(3.45) is the expression of the DC resistance of the winding, however this expression can be adopted because of the use of litz wire. In fact, this kind of wire can reduce significantly the skin effect, so it is possible to assume:

$$R_{DC} \approx R_{AC} \tag{3.47}$$

3.2.3 Transformer design

The procedure used to design the transformer refers to the document "Ferrite and accessories: application notes, TDK" [15].

First of all, the core model must be chosen depending on the power capacity. A suitable solution for a nominal power equal to $11kW$ is *E 100/60/28* ([16], Figure 3.4) and the selected core material is N97 [17], which is characterized by low core losses.

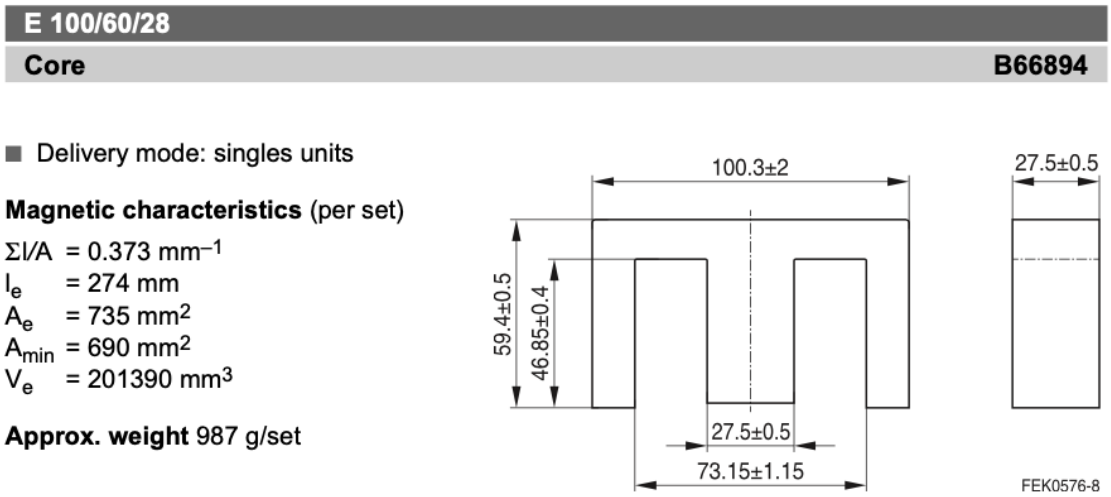

Figure 3.4: TDK Core E 100/60/28

The following relation is used for the calculation of the number of turns on the primary side :

$$V_1 = 4.44 \cdot f \cdot N_1 \cdot B \cdot S_{Fe} \tag{3.48}$$

where:

- $V_1[V]$ is the voltage at the primary side of the transformer
- $f[Hz]$ is the working frequency
- N_1 is the number of turns at the primary side
- $B[T]$ is the magnetic flux density

- $S_{Fe}[m^2]$ is the section of the magnetic path

The following assumptions are considered:

- $V_1 = V_{dc} \cdot M_{max} = 800 \cdot 1.06 = 848V$
- $f = f_{min} = 95346Hz$
- $B = 0.2T$

Moreover, reading the data sheet of the core, the section of the magnetic path is known and it is equal to $S_{Fe} = 690mm^2$. So the number of turns is equal to:

$$N_{prim} = \frac{V_1}{4.44 f_{min} B S_{Fe}} = 19.35 \Rightarrow 20turns \tag{3.49}$$

As the turn ratio of the transformer is equal to 2, the number of turns at the secondary side of the transformer is given by:

$$N_{sec} = \frac{N_{sec}}{n} = \frac{20}{2} = 10turns \tag{3.50}$$

Also for the winding of the transformer, the litz wire is used and the procedure to calculate the sections is similar to the one used for the resonant inductor. From the data sheet of the transformer core, the geometry is know, so it is possible to retrive the total copper section considering a fill factor equal to 0.4:

$$A_{Cu} = \frac{(73.15 - 27.5)}{2} \cdot 2 \cdot 46.85 \cdot 0.4 = 824.4mm^2 \tag{3.51}$$

Assuming that at the secondary side the section of the wires are double with respect to the section at the primary side, the section of the wire at the primary side is given by:

$$S_1 = \frac{A_{Cu}}{N_1 + 2N_2} = \frac{824.4}{40} = 20.61mm^2 \tag{3.52}$$

Consequently, the section at the secondary side is equal to:

$$S_2 = 2S_1 = 41.22mm^2 \tag{3.53}$$

At this point its been decided to use litz wires with nominal section equal to $10mm^2$, so for the primary winding two wires are connected in parallel, while for the secondary side there are four wirese connected in parallel.

As done for the resonant inductor, it is possible to calculate the windings resistance of the transformers:

$$R_{prim} = \rho_{120}\frac{\ell N_{prim}}{S_{Cu,prim}} \tag{3.54}$$

$$R_{sec} = \rho_{120}\frac{\ell N_{sec}}{S_{Cu,sec}} \tag{3.55}$$

where:

- $\rho_{120\Omega mm^2/m} = 0.0244[\Omega mm^2/m]$ is the copper resistivity at $120^{\circ}C$
- $\ell = 208mm$ is the mean length of the turns of the windings
- $N_{prim} = 20turns$ is the number of turns at the primary side
- $N_{sec} = 10turns$ is the number of turns at the secondary side
- $S_{Cu,prim} = 10mm^2$ is the nominal section of the wires at the primary side
- $S_{Cu,sec} = 10mm^2$ is the nominal section of the wires at the secondary side

Substituting these values it is possible to retrive:

$$R_{prim} = 5.1m\Omega \tag{3.56}$$

$$R_{sec} = 1.3m\Omega \tag{3.57}$$

These values can be used also for high frequencies functioning because of the use of litz wire.

3.2.4 Output filter

In order to improve the current waveform at the battery side, an inductor is connected to the output of the LLC converter, forming a CL filter with the output capacitor. The resonance frequency of the output filter is set to $f_{filt} = 10kHz$ which is much less than the minimum switching frequency. A reasonable value of the output inductance in terms of ripple attenuation and size of the inductor is $L_{out} = 10\mu H$. Consequently, the output capacitance is given by:

$$C_{out} = \frac{1}{4\pi^2 f_{filt}^2 L_{out}} = 25\mu F \tag{3.58}$$

Chapter 4

Software simulation

In this chapter the results of the converters design are tested with PLECS simulations. The aim is to check if the parameters found in the last chapters are a good solution for the battery charger and, if not, to choose better values for the application. Moreover, the dynamic of the controlled quantities can be analyzed in order to verify if the parameters of the PI regulators are well tuned.

At first, the two converters are simulated individually to check their functioning and their parameters. During this operation the parameters of the converters have been modified, if required, in order to obtain an optimized design. Before to simulate the complete cascaded converter, the commercial solutions for the converters components are chosen. So the final simulation gives the result of the complete converter behavior with the final chosen parameters and components.

The last section of the chapter is dedicate to the ZVS of the LLC converter. As PLECS does not simulate the switching process, LTSpice will be used for this purpose.

4.1 Simulation of the T-type converter

For the simulation of the T-type converter, the LLC converter is modeled as a current source, which absorb the output power of the T-type converter. The reference value of the DC-link voltage is kept equal to $800V$.

During the simulations, also a grid inductance equal to $100\mu H$ has been taken

into account.

4.1.1 Three-phase configuration

The first simulation of the single-phase T-type converter has been run with the parameters reported in Table 4.1. The parameters of the control and of the PLL

Converter Parameters		
Input Voltage	220	[Vrms]
Switching frequency	20	[kHz]
Input inductance	1.2	[mH]
Output capacitance	3.0	[mF]
Initial capacitor voltage	390	[V]

Table 4.1: Parameters of the T-type converter for the fisrt simulation

are tuned as explained in chapter 3. In order to check the value of the input inductors, the value of the output current source has been set in such a way that the input current of the T-type converter is equal to $16Arms$:

$$I_{out} = \frac{3V_{in}I_{in}}{V_{dc}} = \frac{3 \cdot 220 \cdot 16}{800} = 13.2A \tag{4.1}$$

From this first simulation (Figure 4.1) it is possible to see the following results:

- the currents through in dq coordinates follow their reference values
- the voltage on the DC-link follow its reference value
- the input current has a sinusoidal waveform and it is in phase with the input voltage

Moreover, it is possible to measure the THD of the input current using the cursors inside the PLECS scope. In this case the THD is close to 5% so the value of the input inductance can be decreased. After some tries, the chosen inductance value is $L_{in} = 200\mu H$. Changing the value of the inductance, the new THD value of the input current is equal to 24%. One solution could be to increase the inductance value,

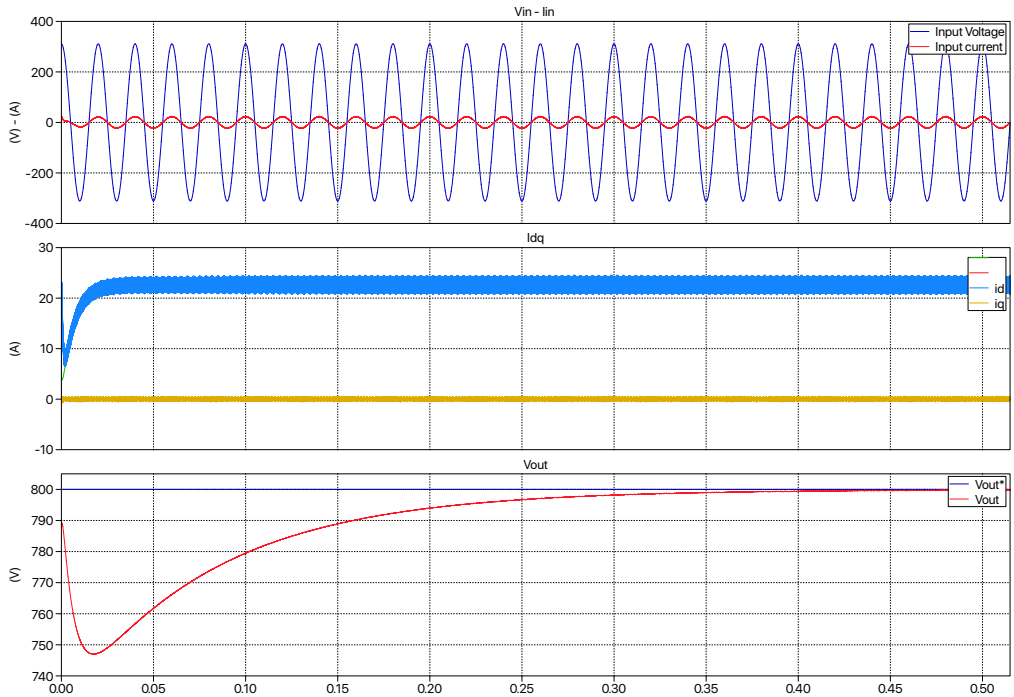

Figure 4.1: Results of the first simulation of the T-type converter

however this will negatively affect the weight and the volume of the converter. An alternative way to overcome the problem is to limit the input current to $16Arms$ so the standard requirements to be satisfied regard just the magnitude of the harmonic components. Limiting the input current does not affect the transferred power so much. The nominal current of the T-type converter should be:

$$I_n = \frac{P_n}{3V_{in}} = \frac{11000}{3 \cdot 220} = 16.67A \tag{4.2}$$

So, limiting the input current to $16A$ does not affect much on the recharging profile and it permits to save weight and volume of the converter.

During the simulation, also the current through the capacitors has been measured:

$$I_{c,rms} = 10.7A \tag{4.3}$$

One simulation has been run at the 10% of the rated power in order to check if the harmonics magnitude of the input currents satisfy the standard requirements. The results (Table 4.2) of the simulation say that the standards are satisfied.

n	f	magnitude	n	f	magnitude
1	50	2.64	21	1050	0.01
2	100	0.19	22	1100	0.01
3	150	0.07	23	1150	0.01
4	200	0.04	24	1200	0.01
5	250	0.33	25	1250	0.01
6	300	0.03	26	1300	0.01
7	350	0.26	27	1350	0.01
8	400	0.02	28	1400	0.01
9	450	0.02	29	1450	0.03
10	500	0.02	30	1500	0.01
11	550	0.10	31	1550	0.02
12	600	0.02	32	1600	0.01
13	650	0.06	33	1650	0.00
14	700	0.02	34	1700	0.01
15	750	0.01	35	1750	0.00
16	800	0.01	36	1800	0.00
17	850	0.02	37	1850	0.01
18	900	0.01	38	1900	0.00
19	950	0.02	39	1950	0.00
20	1000	0.01	40	2000	0.00

Table 4.2: Three-phase T-type converter: Harmonics magnitudes of the input current during a functioning at 10% of the rated power

4.1.2 Single-phase configuration

As the interleaved control reduces the ripple on the inductor currents, the value of inductance found for the three-phase configuration is good also for the single-phase configuration. A simulation at rated power has been run to verify all the components value (Table 4.3) and the tuning of the control parameters, which are

set as described in chapter 3. The results of the simulation (Figure 4.2) lead to the following observations:

Converter Parameters		
Input Voltage	220	[Vrms]
Switching frequency	20	[kHz]
Input inductance	200	[μH]
Output capacitance	3.0	[mF]
Initial capacitor voltage	390	[V]

Table 4.3: Parameters of the single-phase T-type simulation

- the current through the inductor follow their reference value
- the input current has a sinusoidal waveform and it is in phase with the input voltage
- the output voltage follow its reference voltage
- the output voltage is affected by a 100Hz ripple, which peak value is equal to 8V

During the simulations, also the current through the capacitors has been measured. The rms value is a bit higher than in the three-phase configuration and it is equal to:

$$I_{c,rms} = 13.6A \tag{4.4}$$

In order to check if the standard requirements are satisfied also for low values of input current, a simulation has been run at the 10% of the rated power. From the results (Table 4.4) it is possible to see that the standard requirements are satisfied.

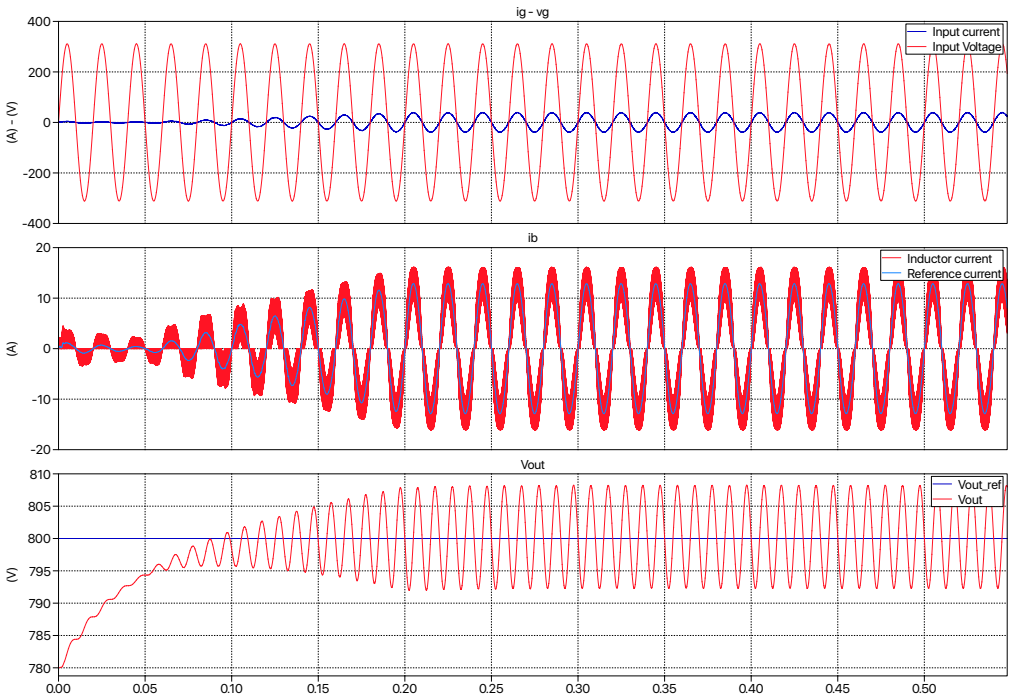

Figure 4.2: Results of the single-phase T-type simulation

4.2 Simulation of the LLC converter

The input of the LLC converter in the simulation is modeled as a constant voltage source, which value is equal to $800V$. In order to consider its dynamic behavior, the battery is modeled as a capacitor with a very high capacitance value. The parameters used for the simulations of the LLC converter are reported in Table 4.5. The regulators are tuned as reported in chapter 3.

As the recharging time is very long, two simulation has been run. The first one starts with an initial battery voltage equal to $350V$ which is the assumed value of the battery voltage when its state of charge is very low. From the first results (Figure 4.3) it is possible to note the following facts:

- at the beginning of the simulation the control does not respond because the LUT needs some moments to find the first frequency value that allow to control the current

n	f	magnitude	n	f	magnitude
1	50	3.86	21	1050	0.01
2	100	0.00	22	1100	0.00
3	150	0.10	23	1150	0.01
4	200	0.00	24	1200	0.00
5	250	0.04	25	1250	0.00
6	300	0.00	26	1300	0.00
7	350	0.07	27	1350	0.01
8	400	0.00	28	1400	0.00
9	450	0.05	29	1450	0.00
10	500	0.00	30	1500	0.00
11	550	0.03	31	1550	0.00
12	600	0.00	32	1600	0.00
13	650	0.02	33	1650	0.00
14	700	0.00	34	1700	0.00
15	750	0.04	35	1750	0.00
16	800	0.00	36	1800	0.00
17	850	0.02	37	1850	0.00
18	900	0.00	38	1900	0.00
19	950	0.01	39	1950	0.00
20	1000	0.00	40	2000	0.00

Table 4.4: Single-phase T-type converter: Harmonics magnitudes of the input current during a functioning at 10% of the rated power

- after the first moments of the simulation, the current follows the reference with a good response
- the reference value of current is saturated to the nominal value
- the voltage at the battery terminals is almost flat because of the the big capacitance value, and it increases very slowly

In order to see the transition from the constant current interval to the constant voltage interval of the charging profile, a second simulation has been run. This time, the initial battery voltage has been set to 415 which is very close to $420V$

Converter Parameters		
Input Voltage	800V	[Vrms]
Resonant inductance	62	$[\mu H]$
Resonant capacitance	40	$[nF]$
Magnetizing inductance	108	$[\mu H]$
Transformer turns ratio	2	[ ]
Filter capacitance	25	$[\mu F]$
Filter inductance	10	$[\mu H]$

Table 4.5: Parameters of the LLC converter used for the simulation

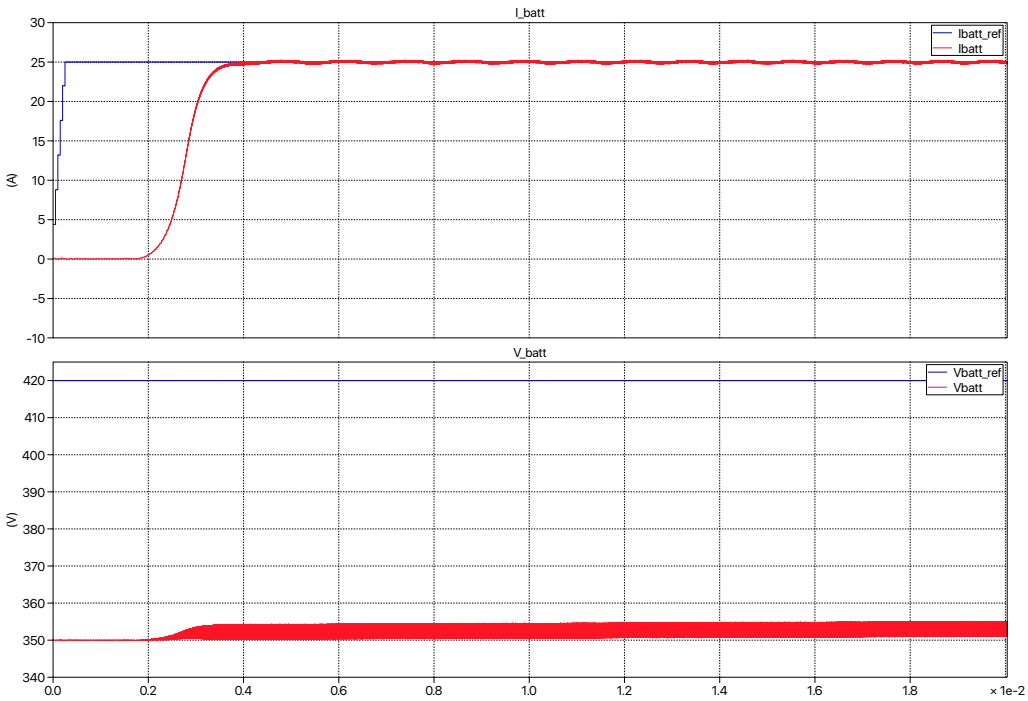

Figure 4.3: Results of the LLC converter simulation with a initial battery voltage equal to 350V

that corresponds to the value of the battery when it is completely recharged. From the results of this second simulation (Figure 4.4), it is possible to note that:

- during the first moments the battery current is equal to the nominal value and

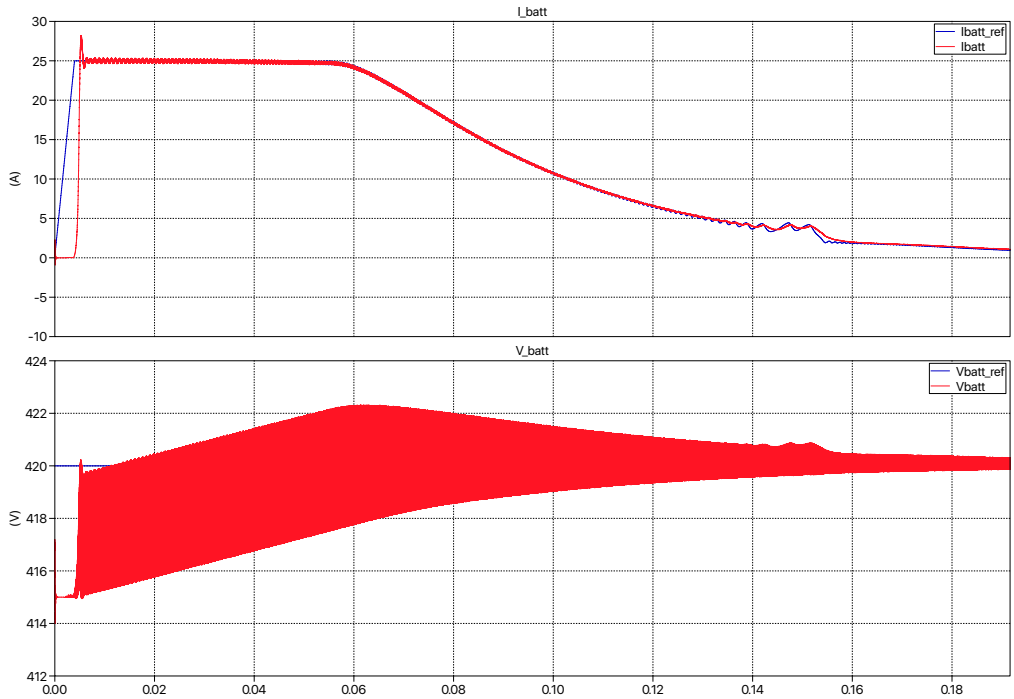

Figure 4.4: Results of the LLC converter simulation with a initial battery voltage equal to 415V

the battery voltage is increasing to reach the desired value

- when the battery voltage reaches the desired value, the current start to decrease and the voltage remain constant: this is the transition between the two intervals of the charging profile
- while the voltage remains constant, the current decreases with time reaching values that are close to zero
- the output voltage is affected by a high frequency ripple, but its magnitude is close to 1% of the nominal value so it is acceptable

Combining the results of the two simulation it is possible to note that the recharging profile correspond to the desired one (Figure 1.9), so the chosen parameters for the converter components and for the PI regulators are suitable for the application.

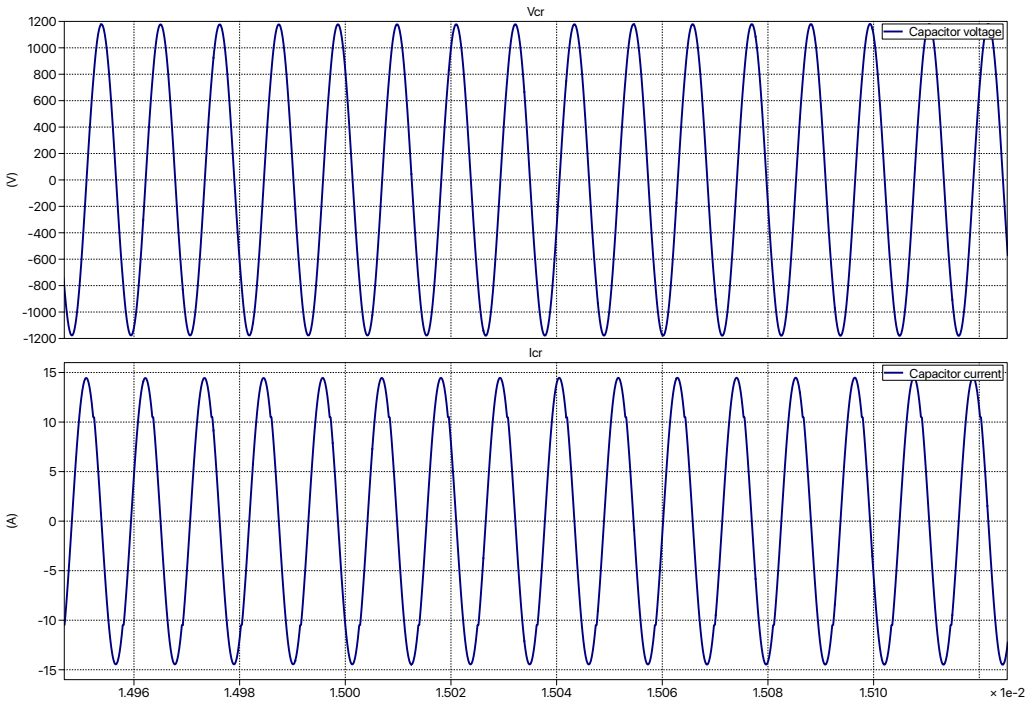

Figure 4.5: Voltage and current of the resonant capacitor during the simulation

During the simulations the value of current through the filter capacitor has been measured and it is equal to:

$$I_{C,filt} = 14.7Arms \tag{4.5}$$

Also the current and the voltage of the resonant capacitor has been measured (Figure 4.5):

$$V_{Cr} = 830Vrms \tag{4.6}$$

$$I_{Cr} = 10.3Arms \tag{4.7}$$

These value are useful in order to choose the commercial solutions for the capacitors.

4.3 Choice of the commercial components

The following list report the relevant values for choosing the commercial solutions of the components:

1. T-type converter

   - Input inductor:

$$L_{in} = 200\mu H \qquad I_n \geq 16A$$

   - Output capacitor:

$$C_{out} = 3mF \qquad I_n \geq 10A \qquad V_n \geq 400V$$

   - Diodes:

$$I_F \geq 16.7A \qquad V_r \geq 800V$$

   - Mosfets:

$$I_F \geq 16.7A \qquad V_r \geq 400V$$

2. LLC converter

   - Resonant capacitor:

$$C_r = 40nF \qquad I_n \geq 10.3 \qquad V_n \geq 830V$$

   - Filter capacitor:

$$C_{out} = 25\mu F \qquad I_n \geq 14.7 \qquad V_n \geq 420V$$

- Mosfets:

$$I_F \geq 7A \qquad V_r \geq 800V$$

- Diodes:

$$I_F \geq 13A \qquad V_r \geq 420V$$

Considering these results, the components has been chosen and the list is reported in Table 4.6. Note that in this section the data sheets of the resonant inductor and of the transformer are not reported because they have already been reported in the last chapter.

T-type converter

Component	Model name	Data sheet
Input inductor	VISHAY IHV	[18]
Output capacitor	259 PHM-SI	[19]
Diode	STPSC20H12-Y	[20]
Mosfet	ST Microelectronics SCTH40N120G2V7AG	[21]

LLC converter

Component	Model name	Data sheet
Resonant capacitor	CalRamic 10HS06N473JS	[22]
Output capacitor	MKP1848 DC-Link	[23]
Output inductor	IHDM-1008BC-30	[24]
Diode	STPSC20H12-Y	[20]
Mosfet	SCT30N120	[25]

Table 4.6: Chosen components for the LLC and T-type converters

The current capability and the rated current of the T-type output capacitor does not satisfy the specification. To overcome the problem it is been decided to

connect four VISHAY 259 PHM-SI in parallel to form one equivalent capacitor. So the T-type converter will have eight capacitors divided into two group. Each group form an equivalent capacitor with the following equivalent capacitance:

$$C_{out,eq} = 4 \cdot 0.68 = 2.72mF \tag{4.8}$$

The result is a bit less then the required value (3mF) so the expectation is an increased value of the ripple at the DC-link terminals.

The value of output capacitance on the LLC converter is a bit higher than $25\mu F$, so the ripple at the battery terminals will be reduced.

4.4 Simulation of the complete converter

The data sheet of the chosen components give all the necessary parameters for the last simulations in which the two converter are connected in order to form the complete battery charger.

Both single-phase and three-phase configurations have been simulated considering the parameters reported in Table 4.7. The initial voltage V_{C0} on the output capacitor of the T-type converter is lower than 400V so it is possible to see if the control of the DC-link voltage works or not. Moreover, the initial voltage of the battery is close to the maximum value because the aim of the simulation is to see the transition between the two recharging intervals.

The simulation with single-phase supply configuration (Figure 4.7) leaded to the following results:

- the input current has a sinusoidal waveform and it is in phase with the input voltage
- the current through the input inductors follow its reference value
- the value of the voltage on the DC-link is initially equal to $2V_{C0}$ and it increases with time until it reaches the reference value
- there is a ripple of 100Hz plus a high freqeuncy ripple on the DC-link voltage: the first one is due to the T-type structure and the second one is due to the

current absorbed by the LLC converter, which is affected by the switching frequency

- the battery current remain at first equal to zero until the LUT find the good value for its control
- after the first moments the battery current follows the reference value
- apart from the switching ripple, the battery current is affected by a 100Hz ripple due to the oscillation of the DC-link voltage
- the battery voltage slowly increases to reach the maximum value and then remain constant
- when the voltage reaches its maximum value, the battery current starts to decrease with time until it reaches values close to zero

The results of the simulation with the three-phase supply configuration (Figure 4.8) are very similar. Just some differences can be highlighted:

- the interval of the recharging profile with constant current is shorter because in this case the battery current is saturated to 25A (15A in the case of the single-phase configuration)
- when the current starts to decrease the voltage on the DC-link increases a little bit because the control bandwidth is not high enough to decrease the input current

The final increasing of the DC-link voltage is not a big problem because its value is very small (1% of the nominal value). Moreover, the time of the simulation is not realistic, in fact in real applications the recharging time take few hours. Consequently, in real situations, the control have time enough to respond to the changing of the battery current, so the DC-link voltage will not increase.

4.5 Simulation of the ZVS in the LLC converter

As mentioned in previous chapters, the LLC converter is employed in order to obtain the ZVS and increasing the global efficiency of the battery charger. The

design made in chapter 4 leaded to the choice of the resonant tank parameters and a simulation of the LLC converter using LTSpice is reported in this section. The result let to understand if the chosen parameters of the resonant tank will really permit the ZVS in the LLC converter. The parameters used in the simulation are reported in Table 4.8.

The aim is to analyze the switching process of the bridge inverter and the time interval of the simulation is very small. Consequently it is possible to consider the output capacitor of the LLC converter as a constant voltage source.

Looking at the turn-off transition (Figure 4.10) it is possible to see that the current through the mosfet decrease significantly before the voltage applied to its terminals reach the value of the input source. The commutation is not perfectly done with zero voltage, but it is a reasonable result and the turn off losses are very low if compared with hard switching converters.

To understand the turn-on transition (Figure 4.11) it is required to look also at the gate signal of the power switch. When the value of the current is negative and the gate signal is still equal to zero it means that the current is flowing through the body diode. When the gate signal switch to one, the voltage at the power switch is already zero, so the ZVS during the turn on is ensured.

T-type converter

f_{sw}	20	$[kHz]$
V_{in}	220	[V]
L_g	100	$[\mu H]$
L_{in}	180	$[\mu H]$
C_{out}	2.70	[mF]
V_{C0}	390	[V]
V_{dc}^*	800	[V]
$\omega_{b,i}$	$2\pi f_{sw} \cdot 0.05$	[rad/s]
$k_{p,i}$	$\omega_{b,i}(L_g + L_{in})$	
$k_{i,i}$	$\omega_{b,i} k_{p,i} \cdot 0.1$	
$\omega_{b,v}$	$0.005\omega_{b,i}$	[rad/s]
$k_{p,v}$	$\omega_{b,i} C_{out}$	
$k_{i,v}$	$\omega_{b,v} k_{p,v} \cdot 0.005$	

LLC converter

L_m	108	$[\mu H]$
L_r	62	$[\mu H$
C_r	47	$[nF]$
n	2	[ ]
C_{out}	40	$[\mu F]$
L_{out}	10	$[\mu H]$
$C_{batt,eq}$	0.5	F
$E_{batt,in}$	416	V
$\omega_{b,i}$	$2\pi f_{sw} \cdot 0.5$	[rad/s]
$k_{p,i}$	$\omega_{b,i} L_{out}$	
$k_{i,i}$	$\omega_{b,i} k_{p,i}$	
$\omega_{b,v}$	$\omega_{b,i} \cdot 0.01$	
$k_{p,v}$	0	
$k_{i,v}$	$\frac{\omega_{b,v}}{R_b}$	

Table 4.7: Parameters for the Simulation of the complete battery charger

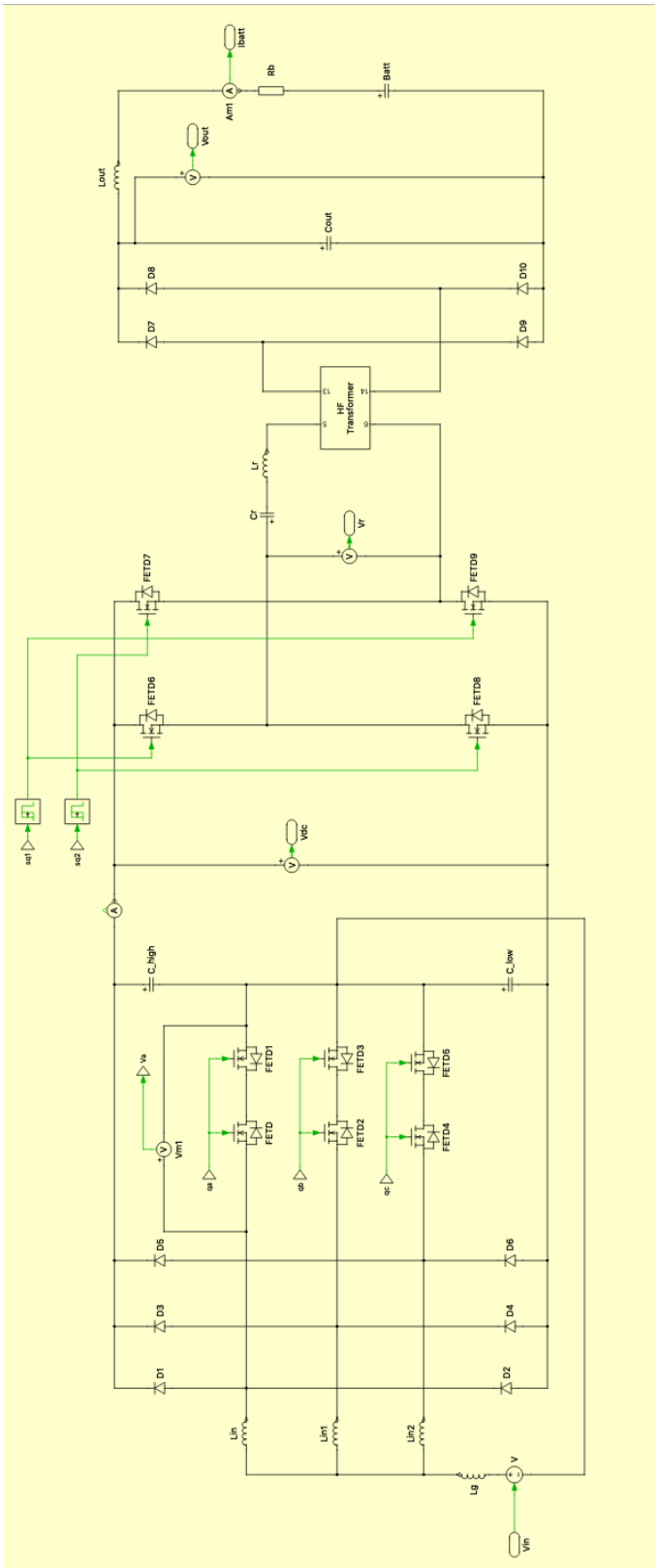

Figure 4.6: Schematic in PLECS of the complete converter with single-phase supply configuration

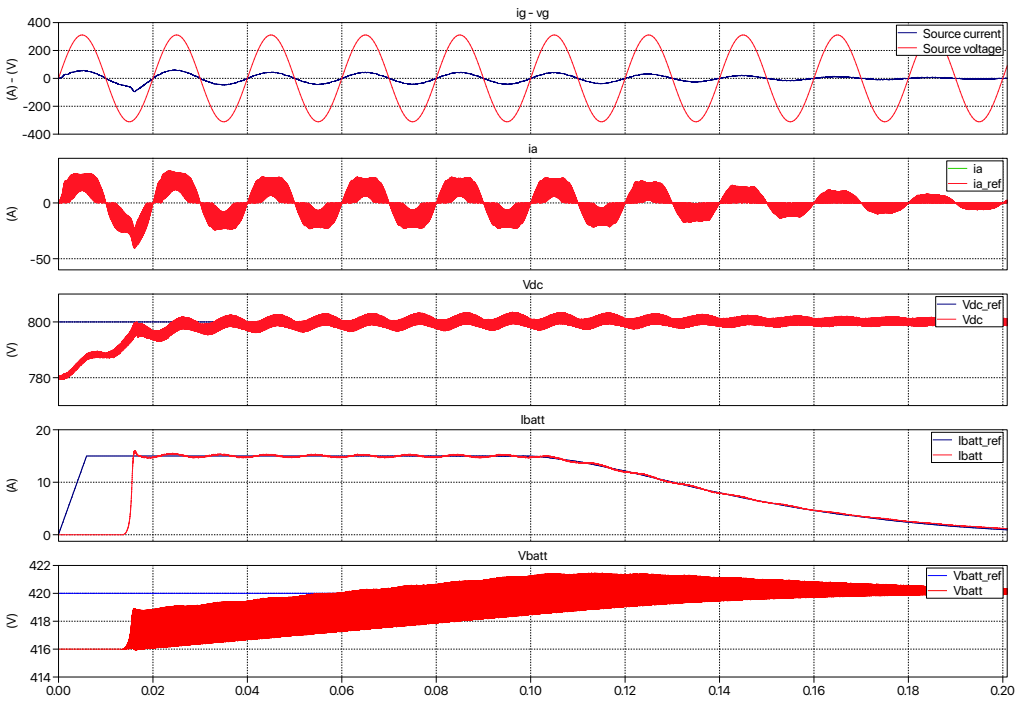

Figure 4.7: Results of the complete battery charger with single-phase supply configuration

V_{in}	800	V
V_{batt}	380	V
L_m	108	$[\mu H]$
L_r	62	$[\mu H$
C_r	47	$[nF]$
n	2	[]
t_{dt}	400	ns
C_{oss}	130	pF

Table 4.8: Parameters of the LLC converter for the simulation in LTSpice

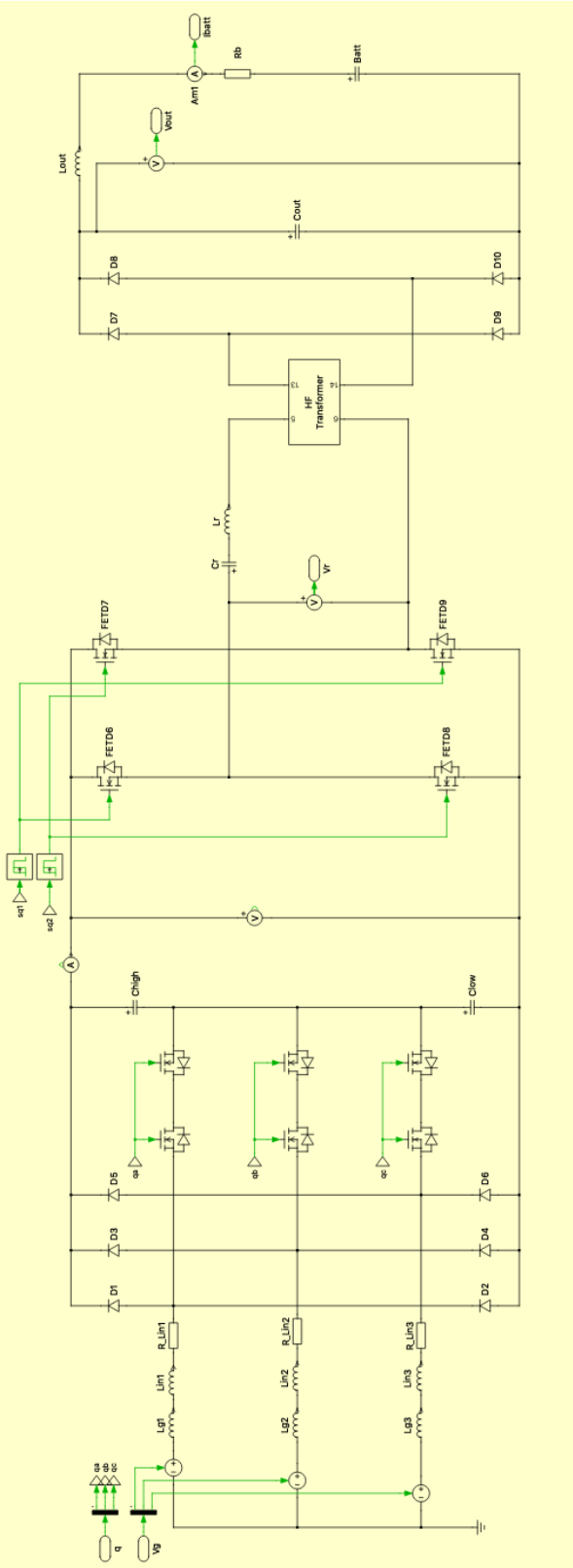

Figure 4.8: Schematic in PLECS of the complete converter with three-phase supply configuration

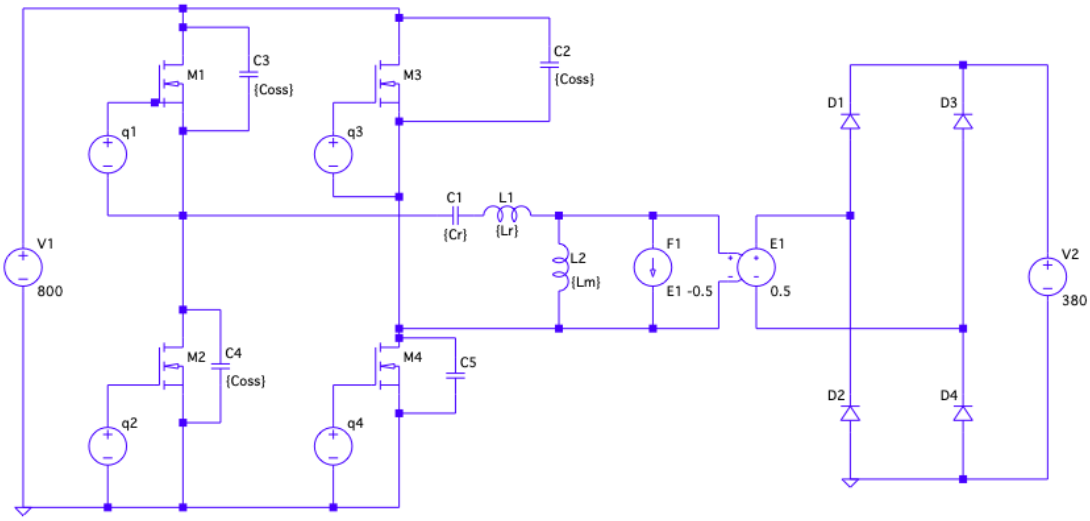

Figure 4.9: Schematic of the LLC converter for the simulation in LTSpice

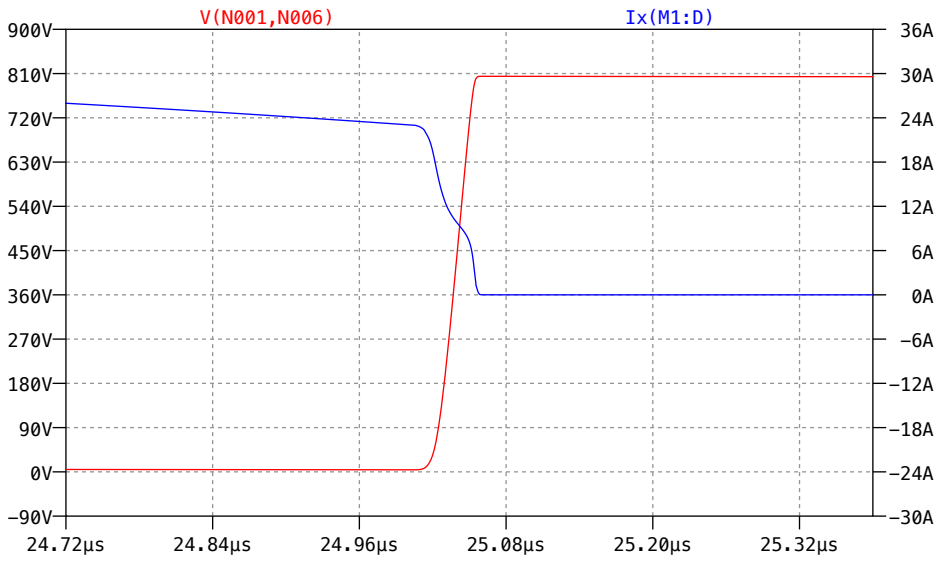

Figure 4.10: Turn-off transition of the power switch in the LLC converter

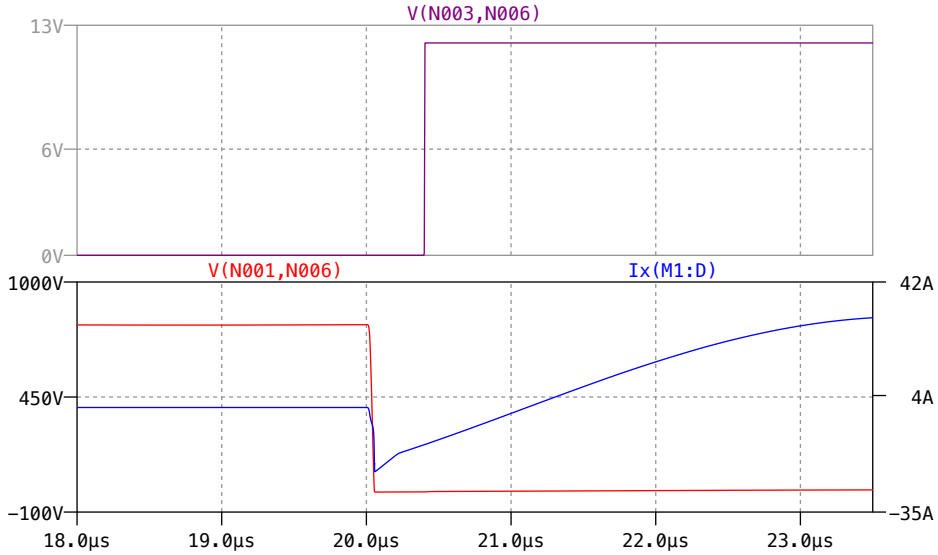

Figure 4.11: Turn-on transition of the power switch in the LLC converter

Chapter 5

Evaluation of weight, volume and losses

In the previous chapters, the components of the battery charger have been determined. Thanks to the data sheets, their dimensions and weight are known and it is possible to draw the rendering of the converter. This will be not necessarily the final configuration of the converter, but it gives an idea on weights and volumes. Using the data provided by the manufacturers of the components used in the battery charger, it is possible also to evaluate the power losses and the efficiency.

Finally, the designed battery charger is compared with a commercial solution.

5.1 Rendering of the battery charger

The various elements of the battery charger are positioned over an aluminum layer that forms the heat sink of the converter. A pipeline passes through the middle part of the heat sink and it permits a heat dissipation through the liquid that flows on its inside. Some space is left above the pipeline in which the power modules will be installed. In this way the heat can be dissipated more efficiently, keeping their temperature at good levels. It should be remarked that, in this work, the heat sink is not sized and it is used just to give a qualitative information about the battery charger footprint.

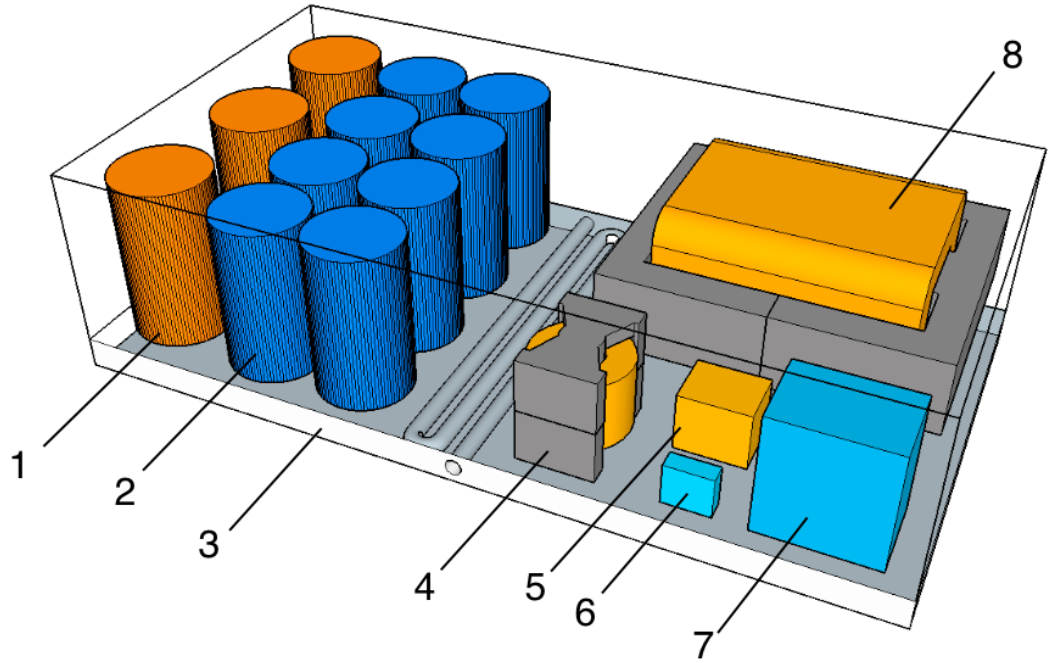

Number	Element	Dimensions [mm]	Weight [g]
1	Input inductor	36×62.23 (D×h)	310
2	DC-link capacitor	35×60 (D×h)	82
3	Aluminum layer	160×11.6×300 (w×h×l)	1503
4	Resonant inductor	36×39.8×41 (w×h×l)	237
5	Output inductor	25×21.7×20.7 (w×h×l)	54
6	Resonant capacitor	17×15×6.8 (w×h×l)	7.27
7	Output capacitor	30×45×42 (w×h×l)	60
8	Transformer	100×60×118.8 (w×h×l)	2400
Total		160×80×300	5848

Figure 5.1: Rendering of the battery charger

5.2 Evaluation of the power losses

The power losses of the battery charger can be evaluated using the data provided by the manufacturer of the components. The calculation requires the measures of currents and voltages inside the converter during its functioning at rated power.

	Single-phase	Three-phase
I_{in}	11.27A	15.67A
I_{Cdc}	16.5A	15.4A
I_r	13.4A	17.33A
I_s	17.46A	28.05A
I_{Cout}	8.73A	13.02A
I_{batt}	15A	25A
V_{prim}	837V	831V

Table 5.1: Measure of the useful quantities for loss calculation at rated powers

Resistance of input inductor	R_{Lin}	21	$m\Omega$
Resistance of the resonant inductor	R_{Lr}	4	$m\Omega$
Resistance of the transformer primary winding	R_{prim}	5.1	$m\Omega$
Resistance of the transformer secondary winding	R_{sec}	1.3	$m\Omega$
ESR of the DC link capacitors	R_{Cdc}	190	$m\Omega$
ESR of the resonant capacitor	R_{Cr}	10	$m\Omega$
ESR of the output capacitor	R_{Cout}	4	$m\Omega$
Resistance of the output inductor	R_{Lout}	2	$m\Omega$
Volume of the transformer core	$V_{core,tr}$	201390	mm^3
Volume of the resonant inductor core	$V_{core,Lr}$	20500	mm^3
Number of winding turns of resonant inductor	N_{Lr}	20	
Number of winding turns at primary side	N_{prim}	20	
Number of winding turns at secondary side	N_{sec}	10	
Nominal core section of the resonant inductor	$S_{Fe,Lr}$	201	mm^2
Nominal core section of the transformer	$S_{Fe,tr}$	735	mm^2

Table 5.2: Parameters of the battery charger used for loss calculations

PLECS have been used for this purpose and the useful quantities for loss calculation are reported in Table 5.1. The parameters of the battery charger components are reported in Table 5.2.

PLECS is also used to evaluate the power losses of the switching elements.

5.2.1 Power losses of the T-type converter

Power losses in the T-typce converter are generated by the following elements:

- *Input inductors.* The working frequency is $50Hz$ and the majority of the losses are caused by Joule effect on the windings so iron losses are negligible:

$$P_{Lin} = 3 \cdot P_{Lin,phase} = 3 \cdot R_{Lin} \cdot I_{in}^2 \tag{5.1}$$

- *Output capacitor.* The loss of power is caused by the current flowing through the ESR. As mentioned in the previous chapter, both equivalent capacitors at the output of the T-type converter are composed of four capacitors connected in parallel, so the equivalent ESR is equal to one fourth of the ESR of one single capacitor. The total power losses on the capacitors is then given by:

$$P_{Cdc} = 2\frac{R_{Cdc}}{4} \cdot I_{Cdc}^2 \tag{5.2}$$

- *Diodes and mosfets.* Both conduction losses and switching losses are considered and they are evaluated using PLECS:

$$P_{mos} = 6(P_{mos,cond} + P_{mos,sw}) \tag{5.3}$$

$$P_{diode} = 6(P_{diode,cond} + P_{diode,sw}) \tag{5.4}$$

The results evaluated for single- and three-phase configuration are reported in Table 5.3

5.2.2 Power Losses of the LLC converter

Power losses in the LLC converter are generated by the following elements:

	Single-phase	Three-phase
P_{Lin}	5.2W	15.5W
P_{Cdc}	26W	34.3W
$P_{mos,cond}$	29.4W	57.5W
$P_{mos,sw}$	2.58W	5.1W
$P_{diode,cond}$	31.56W	40.5W
$P_{diode,sw}$	≈ 0	≈ 0
Total	94.74W	153.35W

Table 5.3: Power losses in the T-type converter at rated power

- *Resonant and output capacitors.* The losses are generated by the current flowing through the ESR

$$P_{Cr} = R_{Cr} \cdot I_r^2 \tag{5.5}$$

$$P_{Cout} = R_{Cout} \cdot I_{Cout}^2 \tag{5.6}$$

- *Resonant inductor and transformer.* As the working frequency is very high, the iron losses can not be neglected:

$$P_{loss} = P_{Cu} + P_{core} \tag{5.7}$$

The power losses due to the Joule effect are given by:

$$P_{Cu} = R_{winding} \cdot I_r^2 \tag{5.8}$$

The core losses are evaluated by considering the relative core losses provided by the manufacturer (Figure 5.2, Figure 5.3) and the volume of the core:

$$P_{core} = P_{core,rel} \cdot V_{core} \tag{5.9}$$

The flux density in the resonant inductor can be retrived by using:

$$B = \frac{L_r \cdot I_r}{N_{Lr} \cdot S_{Fe_Lr}} \tag{5.10}$$

For evaluating the flux density in the transformer it is possible to use instead:

$$B = \frac{V_{prim}}{4.44 \cdot N_{prim} \cdot S_{Fe,tr} \cdot f_{sw}} \tag{5.11}$$

- *Output inductor.* At the output of the LLC converter the electric quantities are DC, so the iron losses are neglected:

$$P_{Lout} = R_{Lout} \cdot I_{batt}^2 \tag{5.12}$$

- *Mosfets.* Thanks to the ZVS, the switching losses of the H-bridge converter can be neglected, only the conduction losses are here considered:

$$P_{mos} \approx P_{mos,cond} \tag{5.13}$$

- *Diodes.* The LLC converter at rated powers work above the first resonant frequency, so the diode of the bridge rectifier are characterized by the ZCS and the power losses due to the switching are neglected:

$$P_{diode} \approx P_{diode,cond} \tag{5.14}$$

- *Resonant inductor.* The resonant inductor works at high frequencies so the core losses must be taken into account. In the previous chapter, the number

The results are reported in Table 5.4. In this case, the denomination "single-phase" and "three-phase" does not concern the configuration of the LLC converter, but the input supply configuration.

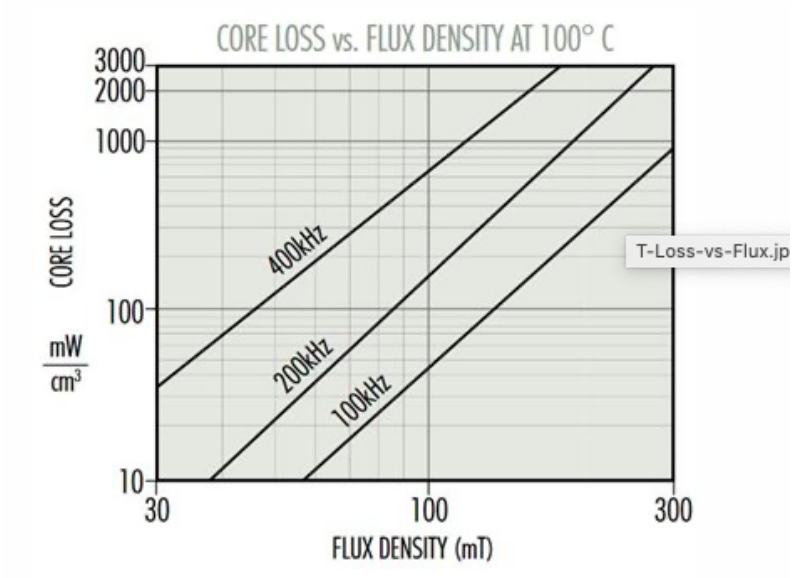

Figure 5.2: Relative core losses of the resonant inductor core

	Single-phase	Three-phase
P_{Lr}	0.72 W	1.6W
$P_{core,Lr}$	4.1W	16.4W
P_{Cr}	1.8W	4W
$P_{tr,prim}$	0.92W	2.04W
$P_{tr,sec}$	0.4W	1W
$P_{core,tr}$	8W	8W
P_{Cout}	0.3W	0.78W
P_{Lout}	0.45	1.25W
$P_{mos,cond}$	60W	124W
$P_{mos,sw}$	≈ 0	≈ 0
$P_{diode,cod}$	44W	113W
$P_{diode,sw}$	≈ 0	≈ 0
Total	120.7W	272.1W

Table 5.4: Power losses in the LLC converter at rated power

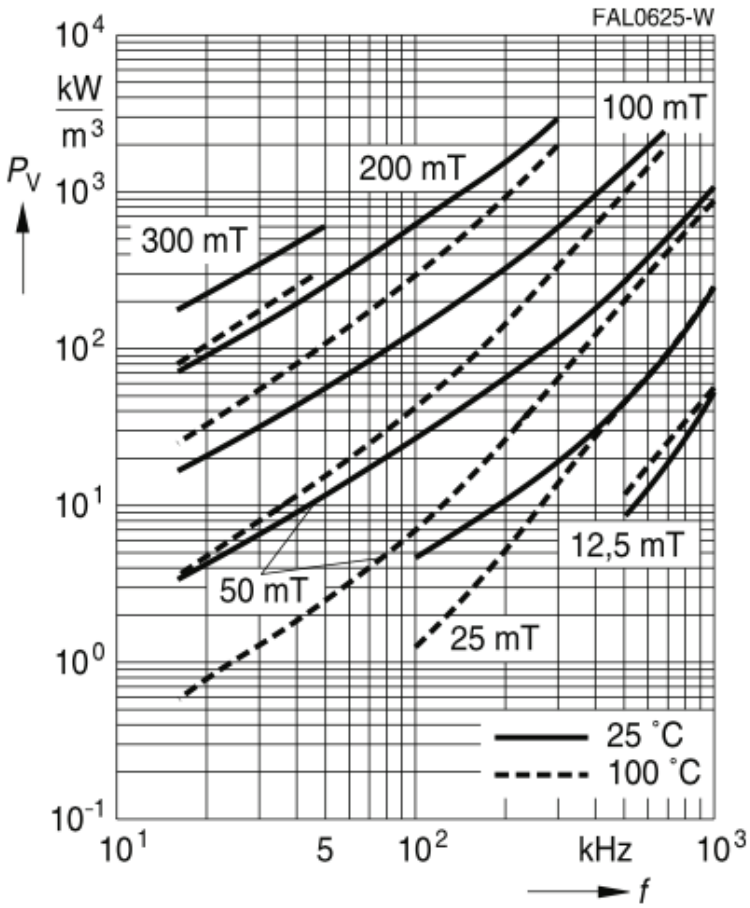

Figure 5.3: Relative core losses of the transformer core [17]

5.3 Efficiency of the battery charger

The total loss of power of the battery charger can be computed using the results of the previous sections:

$$P_{loss} = P_{loss,ttype} + P_{loss,LLC} \tag{5.15}$$

Finally, the efficiency of the battery charger can be retrived by.

$$\eta = \frac{P_{in} - P_{loss}}{P_{in}} = \frac{P_{in} - (P_{loss,ttype} + P_{loss,LLC})}{P_{in}} \tag{5.16}$$

The results are reported in Table 5.5.

	Single-phase	Three-phase
η	96.4%	96.1%

Table 5.5: Efficiency of the battery charger at rated powers.

5.4 Comparison with a commercial solution

Now that all the information about the designed battery charger are known, a comparison can be made considering the BRUSA NLG664 - On Board Fast Charger [26], which mean data are reported in Figure 5.4.

It is possible to see that the weight of the proposed solution is less than one half of the commercial one and also the volume is significantly reduced. This fact can be justified by the double of rated power in three-phase configuration for the commercial solution.

Anyway, the efficiency of the designed battery charger is, at this level of design, higher in both single- and three phase configurations.

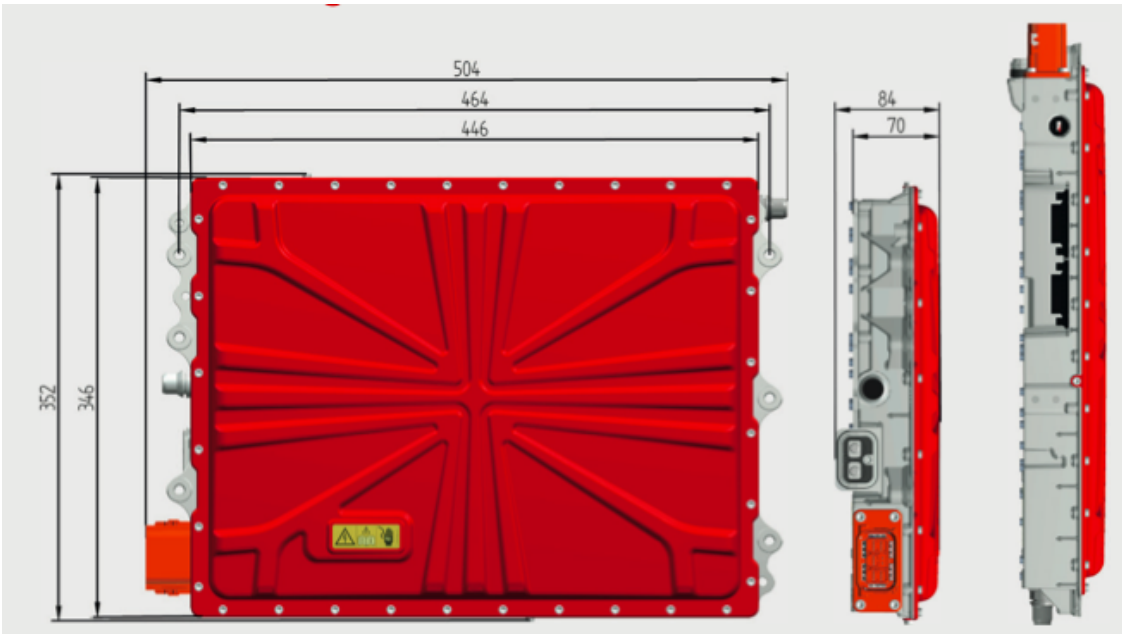

DC output		
Max. charging power three-phase	20.75	kW
Max. charging power single-phase	6.5	kW
Efficiency three-phase	>94	
Efficiency single-phase	>90	
Mechanical Data		
Weight	12	kg
Housing dimensions	352×70×446	mm

Figure 5.4: BRUSA NLG664 - On Board Fast Charger [26]

Chapter 6

Conclusion

this master thesis analyzed and developed an on-board battery charger for electric vehicles that can be used either with single or three-phase input, ensuring a high flexibility in terms of recharging power and input connection.

After analyzing the control strategies the battery charger has been sized and simulated. The results show that the charging profile is ensured for both single- and three-phase configurations. These results demonstrate that the battery charger is able to provide the desired charging power with a high efficiency and low distortion of the grid voltage regardless of the type of input supply system. The developed OBC is able to satisfy the specifications required by the EV and the grid constrains imposed by the standards in terms of power quality regardless the single or three phase configuration. In other words, the battery charger does not create problems in terms of power quality on the grid interface. Moreover, the PFC functioning given by the AC/DC stage permits to absorb currents with an almost unitary power factor.

Finally, the thesis evaluated the feasibility of the OBC by evaluating the weight and volume of each part and with a preliminary rendering of the converter. The aim is to understand if the proposed solution is worth to realize. The the heat sink of the battery charger is not sized in this work and just reasonable values are considered here. However, with the considered assumptions, the proposed battery charger seems to be very compact if compared with other commercial solutions, showing good values in terms of volume and weight of the complete structure.

Last but not least is the analysis of the efficiency. The power losses have been calculated using the data provided by the manufacturers of the various components and, for the semiconductors devices, using PLECS simulations. The results shows an efficiency of about 96% for both single- and three-phase configurations, that is a reasonable result for automotive applications.

To end this discussion, it is possible to say that that the proposed solution shows promising results, so the it can be matter of future studies that aim to develop a more detailed sizing and a physical realization.

Bibliography

[1] A. Khaligh and S. Dusmez. Comprehensive Topological Analysis of Conductive and Inductive Charging Solutions for Plug-In Electric Vehicles. *IEEE Transactions on Vehicular Technology*, 61(8):3475–3489, October 2012.

[2] Nadim Sakr, Daniel Sadarnac, and Alain Gascher. A review of on-board integrated chargers for electric vehicles. *2014 16th European Conference on Power Electronics and Applications*, pages 1–10, August 2014.

[3] CEI. CEI EN 61851-1, 2012.

[4] Dragan Maksimovic Robert W. Erickson. *Fundamentals of Power Electronics - Second edition*. 2001.

[5] Min-Kwon Yang and Woo-Young Choi. Single-phase bidirectional three-level T-type inverter. *2018 IEEE Applied Power Electronics Conference and Exposition (APEC)*, pages 2405–2408, March 2018.

[6] Changsheng Bi, Yanan Shang, Rongbin Lin, Zhiyuan Zhao, Ming Zhou, and Lei Li. Power electronic transformer with ZVS full-bridge phase-shift DC-DC converter. *2017 IEEE Transportation Electrification Conference and Expo, Asia-Pacific (ITEC Asia-Pacific)*, pages 1–4, August 2017.

[7] Christian Oeder and Thomas Duerbaum. ZVS investigation of llc converters based on FHA assumptions. *2013 Twenty-Eighth Annual IEEE Applied Power Electronics Conference and Exposition (APEC)*, pages 2643–2648, March 2013.

[8] Helena Mirante. *Progettazione di convertitori AC/DC per sistemi di ricarica ultrafast delle batterie*. Master thesis, Politecnico di Torino, 2019.

[9] Matteo Gregorio. *Caricabatteria on-board per veicoli elettrici*. Master thesis, Politecnico di Torino, 2018.

[10] Remus Teodorescu, Marco Liserre, and Pedro Rodríguez. *Grid Converters*

for Photovoltaic and Wind Power Systems: Teodorescu/Grid Converters for Photovoltaic and Wind Power Systems. John Wiley & Sons, Ltd, Chichester, UK, 2011.

[11] Toshiba. Resonant Circuits and Soft Switching, 2019.

[12] Enrico Vico. *Design and control of DC-DC converter for ultrafast battery charger for electrical vehicles.* Master thesis, Politecnico di Torino, 2019.

[13] Magnetics. Power Design, 2017.

[14] Magnetics. Core 0T44040UG, 2017.

[15] TDK. Ferrites and accessories - Application notes, May 2017.

[16] TDK. Core E 100/60/28, May 2017.

[17] TDK. Ferrite N97, May 2017.

[18] Vishay. Inductor IHV, 2019.

[19] Vishay. Capacitor 259 PHM-SI, 2018.

[20] ST microelectronics. Diode STPSC20H12-Y, 2019.

[21] ST microelectronics. Mosfet SCTH40N120G2V7AG, 2019.

[22] CalRamic. Capacitor 10HS06N473JS.

[23] Vishay . Capacitor MKP1848, 2019.

[24] Vishay. Inductor IHDM-1008BC-30, 2019.

[25] ST microelectronics. Mosfet SCT30N120.

[26] BRUSA. NLG664 - On Board Fast Charger, 2018.